REPORT DOCUMENTATION PAGE

Form Approved
OMB No. 0704-0188

1. REPORT DATE (DD-MM-YYYY)	2. REPORT TYPE	3. DATES COVERED (From - To)
7-26-2004	Final	1 July 99 - 31 Aug 2003

4. TITLE AND SUBTITLE
Causality Constraints on the Analysis and Active Control of

5a. CONTRACT NUMBER

5b. GRANT NUMBER
N000149911017

5c. PROGRAM ELEMENT NUMBER
G

6. AUTHOR(S)
J. Gregory McDaniel, Cory L. Clarke, Xianhui Li, Xianfeng Zhao

5d. PROJECT NUMBER

5e. TASK NUMBER

5f. WORK UNIT NUMBER

7. PERFORMING ORGANIZATION NAME(S) AND ADDRESS(ES)

The Trustees of Boston University
881 Commonwealth Avenue
Boston, MA 02215

8. PERFORMING ORGANIZATION REPORT NUMBER

9. SPONSORING / MONITORING AGENCY NAME(S) AND ADDRESS(ES)
ONR Regional Office Boston
495 Summer Street Room 627
Boston, MA 02210-2109

10. SPONSOR/MONITOR'S ACRONYM(S)
ONR

11. SPONSOR/MONITOR'S REPORT NUMBER(S)

12. DISTRIBUTION / AVAILABILITY STATEMENT

Approved for Public Release; Distribution Unlimited

13. SUPPLEMENTARY NOTES

14. ABSTRACT

This research has integrated the causality condition into frequency-domain analysis and control of structural vibration, acoustic scattering, and acoustic radiation. As a result of these efforts, a variety of active and passive control approaches are now physically realizable. In the time domain, causality simply requires that a system's response cannot precede its cause. In active control problems, the causality condition further requires that one cannot use future disturbance information to determine control actuation. These conditions are more subtle in the frequency domain, where one typically interprets experimental data and constructs active and passive control approaches. In the frequency domain, the causality condition assumes the form of Hilbert transform relations between elements of the complex Fourier transform of a causal response. This research produced analytical formulations of the causality condition to enhance experimental data and to devise physically realizable control approaches in the frequency domain. Two contemporary active control approaches were used to illustrate the inclusion of causality. The research developed such formulations, and their algorithmic implementations, with a close association to experimental data and control approaches that are of contemporary importance to the Office of Naval Research.

15. SUBJECT TERMS
Structural acoustics, causality

16. SECURITY CLASSIFICATION OF:			17. LIMITATION OF ABSTRACT	18. NUMBER OF PAGES	19a. NAME OF RESPONSIBLE PERSON
a. REPORT	b. ABSTRACT	c. THIS PAGE		75	J. Gregory McDaniel
					19b. TELEPHONE NUMBER (include area code) 617-353-4847

Technical Report
ONR Grant Number N00014-99-1-1017
Causality Constraints on the Analysis and Active Control of Structures

J. Gregory McDaniel
Associate Professor
Department of Aerospace and Mechanical Engineering
Boston University
110 Cummington Street
Boston, Massachusetts 02215
jgm@bu.edu

Graduate Research Assistants:
Cory L. Clarke
Xianhui Li
Xianfeng Zhao

July 26, 2004

Abstract

This research has integrated the causality condition into frequency-domain analysis and control of structural vibration, acoustic scattering, and acoustic radiation. As a result of these efforts, a variety of active and passive control approaches are now physically realizable. In the time domain, causality simply requires that a system's response cannot precede its cause. In active control problems, the causality condition further requires that one cannot use future disturbance information to determine control actuation. These conditions are more subtle in the frequency domain, where one typically interprets experimental data and constructs active and passive control approaches. In the frequency domain, the causality condition assumes the form of Hilbert transform relations between elements of the complex Fourier transform of a causal response. This research produced analytical formulations of the causality condition to enhance experimental data and to devise physically realizable control approaches in the frequency domain. Two contemporary active control approaches were used to illustrate the inclusion of causality. The research developed such formulations, and their algorithmic implementations, with a close association to experimental data and control approaches that are of contemporary importance to the Office of Naval Research.

Contents

List of Figures

Chapter 1

Literature Review

1.1 Causality at Large

The causality condition arises in most time-dependent problems in engineering and physics. The bibliography includes a long list of publications on the causality condition from an astonishingly diverse collection of fields. While detailed review of these publication is beyond the scope of this report, all of this work has been obtained and studied in the course of this project. Many references are cited in the appropriate technical context later in this report.

1.2 Causality and Structural Acoustics

This section offers a detailed review of work involving the causality condition in structural acoustics because this is the focus of the present work. One of the earliest applications was described by Mangulis in a 1963 "Letter to the Editor" [1]. That letter presented Hilbert transform relations between radiation resistance and reactance and illustrated them for the case of a rigid circular piston in an infinite rigid baffle. Mangulis also derived low-frequency behaviors of radiation resistance and reactance. These relations were employed by Radlinski and Meyers [2] in 1974 to explain the frequency dependence of radiation reactance in terms of resonant peaks in the radiation resistance for the case of a pulsating cylinder surrounded by a circular case of parallel cylindrical rods.

Almost two decades passed before the present author began exploring application of these relationships to the design of radiated and scattered sound fields. In a 1993 presentation to the *ONR-Sponsored European Workshop on Structural Acoustics for Young Investigators*, McDaniel [3] presented an approach for deriving structural dynamics that satisfy the causality condition and produce a desired interaction with the surrounding acoustic medium. This work was followed by a 1997 conference paper [4] in which McDaniel investigated two applications of the causality condition to a one-dimensional reflection problem. Both applications employed Hilbert transform relations between the magnitude and phase of a minimum phase system. The first application involved determination of the reflection phase from the magnitude. This is only possible for a minimum phase reflection coefficient, which was found to be equivalent to a reflecting resistance greater than the fluid impedance. The second application involved the determination of a reflecting impedance that produces a specified reflection magnitude. The reflection phase was found by taking the Hilbert transform of the magnitude. The reflecting impedance was found from the usual algebraic relationship between impedance and reflection coefficient. This second application was extended to one-dimensional transmission problems in a 1997 conference presentation by McDaniel [5].

The possibility of deriving reflecting impedances from non-minimum phase reflection coefficients was investigated by McDaniel in 1999 [6]. This work defined a class of reflecting impedances that produce the same reflection magnitudes but different phases. Only one of the impedances produces a minimum phase reflection coefficient. One value of defining such a class is to allow designers to choose the impedances

that are most easily achieved. In following chapters, we review results in two publications that resulted from the present project. The first involved extension of the previous ideas to three-dimensional scattering problems by McDaniel in 2001 [7]. Also during that year, McDaniel and Clarke [8] presented several physical interpretations of minimum phase reflection coefficients and derived a collection of results that allow *a priori* identification of some minimum phase reflection coefficients based on approximate knowledge of the reflecting impedance.

Chapter 2

Mathematical Background

2.1 Introduction

For convenience of referral, this chapter presents mathematical results used in the present work. The notations and conventions of Papoulis [9] are followed as closely as possible and, unless noted otherwise, results in this chapter are from this reference.

2.2 Fourier Transform

A temporal function $f(t)$ and its Fourier transform $F(\omega)$ are related by

$$f(t) = \mathcal{F}^{-1}\{F(\omega)\} = \frac{1}{2\pi}\int_{-\infty}^{\infty} F(\omega)e^{i\omega t}d\omega, \tag{2.1}$$

$$F(\omega) = \mathcal{F}\{f(t)\} = \int_{-\infty}^{\infty} f(t)e^{-i\omega t}dt. \tag{2.2}$$

2.3 Transfer Functions

Consider a linear system with an input $f(t)$ and an output $g(t)$. Then the transfer function is defined as the ratio of the Fourier transforms of output to input,

$$H(\omega) = \frac{G(\omega)}{F(\omega)}. \tag{2.3}$$

If the input is taken as a delta function centered at $t = 0$, $f(t) = \delta(t)$, then its Fourier transform is $F(\omega) = 1$ and (2.3) indicates that the transfer function is the Fourier transform of the response, or $H(\omega) = G(\omega)$. For this reason, the inverse Fourier transform of the transfer function, $h(t)$, is known as the impulse response.

For physical reasons, many impulse responses are required to be real-valued. This requires that the transfer function be conjugate symmetric in frequency,

$$H(\omega) = H^*(-\omega). \tag{2.4}$$

Work presented in this report will frequently involve transfer functions at discrete positive-valued frequencies and the corresponding negative values will be found by invoking the real-valued condition and using the above equation in the frequency domain.

2.4 Definition of the Causality Condition

The causality condition requires that the cause must precede the effect. In linear system theory, this means that the input must precede the output, or simply "no output before input." Therefore, a causal transfer function is one whose impulse response is zero for negative time,

$$h(t) = \mathcal{F}^{-1}\{H(\omega)\} = 0 \text{ for } t < 0, \tag{2.5}$$

because the input is applied at $t = 0$.

2.5 Hilbert Transform

To simplify the presentation of results, the Hilbert transform is defined as

$$\mathcal{H}\{F(\omega)\} = \frac{1}{\pi}\int_{-\infty}^{\infty} \frac{F(\omega)}{\omega - y} dy \tag{2.6}$$

Divergence of the integral at $\omega = y$ is addressed by taking the Cauchy principal value of the integral [10].

2.6 Relationships Between Real and Imaginary Parts

Writing the transfer function as $H(\omega) = H_{re}(\omega) + iH_{im}(\omega)$, causality requires that

$$H_{im}(\omega) = -\mathcal{H}\{H_{re}(\omega)\}, \tag{2.7}$$
$$H_{re}(\omega) = H_{re}(\infty) + \mathcal{H}\{H_{im}(\omega)\}. \tag{2.8}$$

A proof of the above relations, which are central to the present work, is outlined here. The impulse response, $h(t)$, is written as a sum of even and odd parts, $h(t) = h_e(t) + h_o(t)$. This is always possible by defining

$$h_e(t) = [h(t) + h(-t)]/2, \tag{2.9}$$
$$h_o(t) = [h(t) - h(-t)]/2. \tag{2.10}$$

If $h(t)$ is zero for negative time, then even and odd parts are related by the sign function,

$$h_o(t) = h_e(t)\text{sgn}(t), \tag{2.11}$$
$$h_e(t) = h_o(t)\text{sgn}(t), \tag{2.12}$$

so that the sum of even and odd parts is zero for negative time and twice either part for positive time. Noting the Fourier transform pairs

$$h_e(t) \longleftrightarrow H_{re}(\omega), \tag{2.13}$$
$$h_o(t) \longleftrightarrow iH_{im}(\omega), \tag{2.14}$$
$$\text{sgn}(t) \longleftrightarrow \frac{2}{i\omega}, \tag{2.15}$$

the Fourier transform of (2.11) and (2.12) is

$$iH_{im}(\omega) = H_{re}(\omega) * \frac{2}{i\omega}, \tag{2.16}$$
$$H_{re}(\omega) = iH_{im}(\omega) * \frac{2}{i\omega}. \tag{2.17}$$

Inserting the definition of frequency-domain convolution into the above two equations yields the Hilbert transforms in (2.7) and (2.8). The constant $H_{re}(\infty)$ accounts for singularities in $h(t)$ at $t = 0$.

2.7 Relationships Between Magnitude and Phase

Relationships between magnitude and phase are derived by first assuming that $H(\omega)$ is assumed causal, so it cannot have poles in the lower-half of the complex frequency plane. This is because the evaluation of the inverse Fourier transform for negative times would require a contour in the lower half of the complex frequency plane. Next, assume that $H(\omega)$ has no zeros in the lower half of the complex frequency plane so that its logarithm is also causal. This is known as the minimum phase condition and it will be explored in detail below. Writing the transfer function in terms of the magnitude $\alpha(\omega)$ and phase $\theta(\omega)$,

$$H(\omega) = \exp\{-\alpha(\omega) - i\theta(\omega)\}, \tag{2.18}$$

allows the negative of its logarithm to be expressed as

$$-\ln H(\omega) = \alpha(\omega) + i\theta(\omega),. \tag{2.19}$$

The function $-\ln H(\omega)$ is causal, which allows $\alpha(\omega)$ and $\theta(\omega)$ to be related according to (2.7) and (2.8),

$$\theta(\omega) = -\mathcal{H}\{\alpha(\omega)\} \tag{2.20}$$

$$\alpha(\omega) = \alpha(\infty) + \mathcal{H}\{\theta(\omega)\} \tag{2.21}$$

2.8 Interpretations of the Minimum Phase Condition

One interpretation of the minimum phase condition, which is accepted by many as the definition, is that $H(\omega)$ may not have zeros in the lower half of the complex frequency plane [9]. This condition insures that the system's inverse transfer function is also causal because $H^{-1}(\omega)$ will have no poles in the lower plane if $H(\omega)$ has no zeros there [11]. The inverse impulse response, $\mathcal{F}^{-1}\{H^{-1}(\omega)\}$, is only causal when $H(\omega)$ is minimum phase. Zeros in the lower half of the complex frequency domain create phase shifts in the transfer function as frequency is varied along the real axis, which is the hallmark of a nonminimum phase function. In particular, passing beneath a zero in the lower half of the plane creates a phase shift of $(-\pi)$ [12]. One can show that as frequency is varied from ∞ to 0, a nonminimum phase function experiences a greater positive phase shift than a minimum phase function with the same magnitude. This is the source of the *minimum phase* adjective [13].

Further insight into the minimum phase condition may be gained by expressing a nonminimum phase transfer function as a product of a minimum phase function, H_{mp}, and an all-pass function H_{ap}, according to [14]

$$H_{nmp}(\omega) = H_{ap}(\omega)H_{mp}(\omega). \tag{2.22}$$

Each of the two functions on the right must satisfy the causality and real-valued conditions. In addition, the all-pass function must have a unit magnitude at all frequencies,

$$|H_{ap}(\omega)| = 1. \tag{2.23}$$

Therefore, each nonminimum phase function has an associated minimum phase function that has the same magnitude but a different phase.

One useful form of the all-pass function is given by Victor [14],

$$H_{ap}(\omega) = e^{i\omega D}\prod_j P(\omega, u_j). \tag{2.24}$$

The exponential term is recognized as a time shift D that creates a pure delay in response. For simplicity, we shall henceforth assume that time has been referenced to the first occurence of an output signal, so that $D = 0$. The factors are defined as

$$P(\omega, u_j) = \frac{\omega - u_j}{\omega - u_j^\star}. \tag{2.25}$$

These factors and their product are sometimes referred to as the Blaschke factors and product [15]. In order for H_{ap} to satisfy the causality and real-valued conditions, the Blaschke product must be carefully chosen. To satisfy the causality condition, the poles should be in the upper plane. This requires that $\Im\{u_j\} < 0$. To satisfy the real-valued condition, the Blaschke product must have the property indicated in Equation 2.4,

$$\prod_j P(\omega, u_j) = \prod_j P^\star(-\omega, u_j). \tag{2.26}$$

This may be achieved by either choosing the Blaschke factors in pairs of the form $P(w, u_j)$ and $P(w, u_k)$, where $\Re\{u_j\} = -\Re\{u_k\}$, or by requiring a single factor to have a pure imaginary u_j.

Time-domain descriptions of the minimum phase condition have received less attention in the literature but are interesting and useful. The present work shall explore a description that was presented by Eisner [16] and involves the output energy of the system. Suppose that the integrated energy in the impulse response up to time T is given as

$$E_h = \int_0^T |h(t)|^2 \, dt. \tag{2.27}$$

Next, suppose that $H(\omega)$ is multiplied by a causal all-pass function, $H_{ap}(\omega)$, and the resulting time-domain response is $g(t)$. Then Parseval's Theorem may be used to prove the inequality

$$E_h \geq E_g. \tag{2.28}$$

This implies that any multiplication by an all-pass function has the effect of decreasing the energy that has arrived up to a T. The key implication of this result for the present work is that the response energy in a minimum phase system integrated up to time T is greater than that of a nonminimum phase system with the same frequency-domain magnitude.

Chapter 3

Expansions of Transfer Functions

3.1 Implicitly causal expansions

Analytical formulations of the causality condition that are used in later chapters are based on the following identities [17]:

$$\mathcal{H}\{\sin(\omega t)\} = -\cos(\omega t), \tag{3.1}$$

$$\mathcal{H}\{\cos(\omega t)\} = \sin(\omega t). \tag{3.2}$$

The causality conditions in (2.7) and (2.8) are identically satisfied by the following Fourier series expansion of a transfer function:

$$H(\omega) = \sum_{n=0}^{N} h_n \exp\left(\frac{-in\pi\omega}{\Omega}\right) \tag{3.3}$$

over a frequency band $\omega_0 \leq \omega \leq (\omega_0 + 2\Omega)$. We shall refer to this series as *implicitly causal* because it is causal for any choice of complex-valued Fourier coefficients. A direct verification that this series satisfies the causality condition requires an inverse Fourier transform to obtain the impulse response, which is

$$h(t) = \sum_{n=0}^{N} h_n \delta\left(t - \frac{n\pi}{\Omega}\right). \tag{3.4}$$

This is an evenly spaced series of delta functions that begins at $t = 0$ and ends at $t = N\pi/\Omega$. Since (3.3) is only required to represent the function over a range of positive frequencies, the real-valued condition may be automatically satisfied by using (2.4) to define the transfer functions at negative frequencies. The series in (3.3) was used by Sarkar [18], and it is equivalent to a numerical evaluation of the Hilbert transform by Fourier transform methods [10, 19].

3.2 Implicitly causal and minimum phase expansions

This approach may be used to derive an implicitly minimum phase and causal series, which we have not found in the open literature. This extension is derived from a causal Fourier series for the natural logarithm of the transfer function,

$$\ln H(\omega) = \sum_{n=0}^{N} h_n \exp\left(\frac{-in\pi\omega}{\Omega}\right) \tag{3.5}$$

Taking the exponent of both sides yields an implicitly causal and minimum phase expansion,

$$H(\omega) = \exp\left[\sum_{n=0}^{N} h_n \exp\left(\frac{-in\pi\omega}{\Omega}\right)\right] \tag{3.6}$$

Chapter 4

Interpretation and Identification of Minimum Phase Reflection Coefficients

If the acoustic reflection coefficient is minimum phase, then the causality condition can be used to reconstruct its phase from its magnitude. Such reconstructions are useful when environmental conditions obscure the phase, which is vital to understanding the dynamics of the reflecting object. However, the reconstructions are usually impossible because one cannot be sure that the reflection coefficient is minimum phase. The present work addresses this difficulty by formulating a time-domain description of the minimum phase condition and by identifying classes of submerged objects that always create minimum phase reflection coefficients. Numerical examples are used to confirm the analytical findings and to illustrate their applicability to objects that reflect sound with a wide range of magnitudes.

4.1 Introduction

It is often the case in experiments and sensing activities that the magnitude of a reflected or transmitted acoustic wave is more easily measured than its phase. While the magnitude can be accurately estimated from suitable time averages, ambient noise as well uncertainties in target and receiver locations conspire to contaminate the phase over broad frequency bands. These factors typically leave the experimentalist with nothing but an accurately measured reflection coefficient magnitude over the frequency range of interest. If the phase of the reflection coefficient was known, the complex valued reflection coefficient could be used to determine dynamics properties of the object that enhance its identification. For this reason, the present work is concerned with the finding of a reflection coefficient phase from its magnitude using causality.

Recently, the problem of recovering nonminimum phase from the magnitude of a transfer function has received increased attention. Sarkar [18] presented a method that relies on a Fourier series expansion of the real and imaginary parts of the transfer function. The Fourier coefficients are initially chosen by recovering the minimum phase and are then iteratively adjusted so that the magnitude of the transfer function matches a measured value. While this technique is useful in examples involving the antenna radiation-power patterns and microwave filters, it does not produce correct results for the structural acoustics problems considered here. The fundamental reason is that the reflection coefficient phase does not exhibit the same frequency characteristics as the phases in the electromagnetic examples considered by Sarkar.

The causality condition has been used to relate portions of transfer functions that arise in acoustic radiation problems. Such problems are often characterized by the frequency-dependent radiation impedance of a wetted surface, defined here as the ratio of surface pressure to velocity. Causality may be generally used to relate the real and imaginary parts of this transfer function, as was first suggested by Mangulis [1] and

used by Radlinski [2]. In these applications, the causality condition requires that an acoustic pressure on the surface cannot be produced until it acquires a nonzero velocity.

The one-dimensional acoustic reflection and transmission problems considered here are more complex than the radiation problem previously considered because they typically involve two transfer functions. The first is the mechanical impedance of the object, defined here as the ratio of applied force to velocity. For this transfer function, causality requires that the object cannot apply a stress to the fluid at its wetted surface until it acquires a velocity. The second transfer function is the reflection coefficient, defined here as the ratio of the reflected wave amplitude to the incident wave amplitude. Here, causality requires that waves may not be reflected from an object before an incident wave arrives. Since the object impedance and the reflection coefficient are algebraically related, causal impedances produce causal reflection coefficients. These ideas were first explored by McDaniel [6] for one-dimensional acoustic reflections from mass-spring-dashpot systems.

The first goal of this chapter is to interpret the minimum phase condition for the reflection of a plane wave normally incident on an impedance surface. This is achieved by reviewing existing descriptions of the minimum phase condition, which was done in the previous section, and describing a new time-domain interpretation. The second goal is to identify two classes of submerged objects that produce minimum phase reflection coefficients. The first class consists of objects that effectively transfer velocity and the second class consists of objects that effectively transfer force.

4.2 A Response-Based Description of the Minimum Phase Condition

In this section, a time-domain description of the minimum phase condition is presented that complements the descriptions in the previous section by giving physical insight into the time-domain response of nonminimum phase functions. For clarity, the discussion begins with a simple form of the all-pass function in Equation 2.24. Following discussion of this example, a generalization is presented.

Consider a single Blaschke factor,

$$H_{ap}(\omega) = \frac{\omega - u}{\omega - u^*}. \tag{4.1}$$

The real-valued condition in (2.4) leads to the condition that u be pure imaginary. Writing $u = iu_i$, the function is expressed as

$$H_{ap}(\omega) = 1 - u_i \frac{2u_i - i2\omega}{u_i^2 + \omega^2}. \tag{4.2}$$

When this function is transformed to the time domain by (2.1), the following simple form results [20]:

$$h_{ap}(t) = \begin{cases} 0 & t < 0 \\ \delta(t) - 2u_i e^{-u_i t} & t \geq 0 \end{cases}. \tag{4.3}$$

The frequency-domain multiplication of the all-pass and minimum phase functions in (2.22) amounts to a convolution in the time domain,

$$h_{nmp}(t) = h_{ap}(t) * h_{mp}(t) \tag{4.4}$$

Using Equation 4.3, the nonminimum phase impulse response is

$$h_{nmp}(t) = h_{mp}(t) - 2u_i \left[e^{-u_i t} * h_{mp}(t) \right]. \tag{4.5}$$

Therefore, the nonminimum phase response is a sum of the minimum phase response and the response of the minimum phase system to an additional exponential forcing function.

Generalization of this result to the general case is conceptually straightforward. The all-pass function in (2.24) is cast in the form

$$H_{ap}(\omega) = 1 - H_{rem}(\omega). \tag{4.6}$$

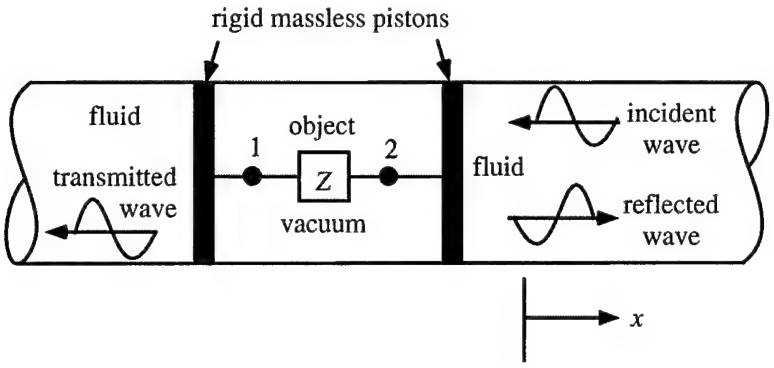

Figure 4.1: A schematic of the one-dimensional reflection and transmission of acoustic waves by a passive linear object.

Substituting (4.6) into (2.22) gives

$$H_{nmp}(\omega) = H_{mp}(\omega) - H_{mp}(\omega)H_{rem}(\omega). \tag{4.7}$$

or, in the time domain,

$$h_{nmp}(t) = h_{mp}(t) - h_{rem}(t) \star h_{mp}(t). \tag{4.8}$$

These results indicate that the nonminimum phase impulse response is the sum of the equivalent minimum phase impulse response and the response of the minimum phase system to a forcing function of $h_{rem}(t)$.

It is interesting to note that this forcing function, $h_{rem}(t)$, is causal and real-valued. One may observe the real-valued property by evaluating the real and imaginary parts of (4.6) at negative and positive frequencies. These evaluations lead to

$$H_{rem}(\omega) = H^{\star}_{rem}(-\omega). \tag{4.9}$$

The remainder function is recognized as causal by taking the inverse Fourier transform of (4.6),

$$h_{rem}(t) = \delta(t) - h_{ap}(t). \tag{4.10}$$

Because $\delta(t)$ and $h_{ap}(t)$ are both causal, $h_{rem}(t)$ must be causal.

4.3 A Minimum Phase Condition for the Reflection Coefficient

In this and the following sections, the minimum phase condition is explored for the reflection coefficient of a passive object immersed in an infinite waveguide. For clarity, the one-dimensional problem shown in Figure 4.1 will serve as the basis for discussion. In this figure, the object is positioned in an infinite waveguide of cross-sectional area A that contains a fluid with sound speed c and mass density ρ. Forces are transmitted between the object and the fluid via two rigid massless pistons. The object is insonified by an incident wave, creating reflected and transmitted waves that propagate away from the object.

In the frequency domain, the dynamic properties of the object are completely described by an impedance matrix that relates forces and velocities at the ports labelled 1 and 2 in the figure according to

$$\left\{ \begin{array}{c} F_1(\omega) \\ F_2(\omega) \end{array} \right\} = \left[\begin{array}{cc} Z_{11}(\omega) & Z_{12}(\omega) \\ Z_{21}(\omega) & Z_{22}(\omega) \end{array} \right] \left\{ \begin{array}{c} V_1(\omega) \\ V_2(\omega) \end{array} \right\}, \tag{4.11}$$

where F_1 and F_2 are the forces applied to the object by the fluid in the directions of the velocities V_1 and V_2, all of which are defined as positive in the x direction. Reciprocity requires the impedance matrix to be symmetric, so that $Z_{12}(\omega) = Z_{21}(\omega)$. The effective impedance seen by the incident wave is simply $Z_{eff} = F_2/V_2$.

This effective impedance is found by noting equal and opposite forces between the object and the fluid at port 1 and by noting that the fluid to the left of the object requires the ratio $F_1/V_1 = -Z_{fl}$, where $Z_{fl} = \rho cA$. Algebraic combination of this result with (4.11) gives the effective impedance seen by the incident wave,

$$Z_{eff} = Z_{22} - \frac{Z_{12}^2}{Z_{11} + Z_{fl}}. \tag{4.12}$$

The effective impedance is the drive-point impedance presented by the object and the fluid to the left of the object if the fluid to the right of the object were removed. It has been shown that the drive-point impedance of any linear system, electrical or mechanical, belongs to a class of "positive real" functions [21, 9]. These functions possess many interesting properties, but the most important to the present discussion is that the real part of a positive real function is positive in the lower half of the complex frequency plane and on the real frequency axis. This property, which is a direct consequence of causality and passivity, will be used in the following sections to identify minimum phase reflection coefficients for two special cases.

When an incident wave of unit amplitude strikes the object, a reflected wave is created that propagates away from the object. The acoustic pressure in the fluid due to this reflected wave is

$$P_r(\omega, x) = R(\omega)e^{ik(\omega)x}, \tag{4.13}$$

where R is the reflection coefficient and $k = \omega/c$ is the acoustic wavenumber. Continuity of force and displacement at the right-hand piston face yields an algebraic relationship between the reflection coefficient and the effective impedance [22],

$$R(\omega) = \frac{z_{eff}(\omega) - 1}{z_{eff}(\omega) + 1}, \tag{4.14}$$

where the normalized effective impedance is

$$z_{eff}(\omega) = Z_{eff}(\omega)/(\rho cA). \tag{4.15}$$

The reflection coefficient is minimum phase when it has no zeros in the lower half of the complex frequency plane. One means of satisfying this condition is to require the real part of the numerator to be strictly positive or negative in this region, so that it cannot pass through a zero. If either

$$\Re\{z_{eff}(\omega)\} > 1 \text{ for } \Im\{\omega\} \leq 0 \tag{4.16}$$

or

$$\Re\{z_{eff}(\omega)\} < 1 \text{ for } \Im\{\omega\} \leq 0, \tag{4.17}$$

then R is minimum phase. Evaluation of these criterion requires a detailed knowledge of the generally complex-valued impedance matrix. In the envisioned applications, where only the magnitude of the reflection coefficient is measured, one usually knows very little about the impedance matrix and the above criterion are not helpful. This difficulty is overcome in the special cases described in the following two sections.

Before considering these special cases, let us develop some additional physical intuition of the minimum phase condition on the reflection coefficient by specializing the time-domain descriptions presented in the previous two sections. The reflection coefficient may be interpreted as the Fourier transform of the reflected pressure due to an incident wave that applies a Dirac pressure distribution to the object at time $t = 0$. Since the magnitude of the acoustic intensity vector for a plane wave is $I = p^2/(\rho c)$, the energy quantity defined in Equation 2.27 is proportional to the integrated acoustic energy that has left the object up to time T. Therefore, an object with a minimum phase reflection coefficient has the property of reflecting the acoustic energy faster than an object with the same magnitude of reflection coefficient but with a nonminimum phase.

The response-based description of the minimum phase property presented in the previous section also provides a physical basis for interpreting the reflection coefficient. In particular, Equation 4.8 can be applied to the reflection problem by interpreting h_{nmp} as the pressure reflected by a nonminimum phase object. This pressure is a sum of two terms. The first is identified as the pressure reflected when a Dirac incident wave insonifies a minimum phase object with the same reflection coefficient magnitude. The second term is the pressure radiated by the same minimum phase object when forced by a pressure distribution of $-h_{rem}(t)$ applied to the object.

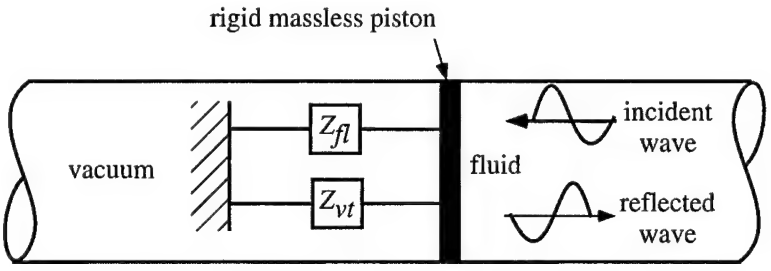

Figure 4.2: A schematic of the system in Figure 4.1 under the assumption that the object perfectly transmits velocity.

4.4 Systems with Perfect Velocity Transfer

In this section, the reflection coefficient is shown to be minimum phase when the velocities at points 1 and 2 in Figure 4.1 are equal. This situation is sometimes referred to as "perfect velocity transfer." While it is tempting to interpret this as a rigid body condition, one must bear in mind that the object may have internal degrees-of-freedom due to internal inertia and flexibility. The condition of perfect velocity transfer only requires that the boundary velocities at points 1 and 2 are equal. One example of such an object would be a very stiff container with an assemblage of masses, springs, and dashpots inside.

In order to understand the conditions that lead to perfect velocity transfer, Equation 4.11 is inverted to the form

$$\left\{ \begin{array}{c} V_1(\omega) \\ V_2(\omega) \end{array} \right\} = \left[\begin{array}{cc} Y_{11}(\omega) & Y_{12}(\omega) \\ Y_{21}(\omega) & Y_{22}(\omega) \end{array} \right] \left\{ \begin{array}{c} F_1(\omega) \\ F_2(\omega) \end{array} \right\}, \tag{4.18}$$

where the admittance matrix is the inverse of the impedance matrix, $[Y] = [Z]^{-1}$. Equating the velocities leads to the condition

$$(Y_{11} - Y_{12})F_1 = (Y_{22} - Y_{12})F_2 \tag{4.19}$$

For this equation to hold for arbitrary frequency-dependent forces, every element in the admittance matrix must be identical so that

$$[Y] = \left[\begin{array}{cc} Y_{vt} & Y_{vt} \\ Y_{vt} & Y_{vt} \end{array} \right], \tag{4.20}$$

where the subscripted vt denotes the assumed "velocity transfer" property of the object. Substitution of this result into Equation 4.18 yields the simple relation

$$F_{net} = Z_{vt}V, \tag{4.21}$$

where the net force acting on the object is $F_{net} = F_1 + F_2$ and V is either V_1 or V_2. The velocity transfer impedance is simply $Z_{vt} = 1/Y_{vt}$. This impedance acts in parallel to the acoustic impedance of the fluid to the left of the piston because the velocities of the fluid and the object are identical.

A schematic of the reduced system is shown in Figure 4.2. The normalized effective impedance defined by Equations 4.12 and 4.15 is simply

$$z_{eff} = 1 + z_{vt}. \tag{4.22}$$

Now, we use the previously quoted result that the drive-point impedance, z_{vt}, of a passive linear system is a positive real function. Its real part is always positive in the lower half of the complex frequency plane and the real part of z_{eff} is always greater than unity. Therefore, the condition in Equation 4.16 is met and the reflection coefficient is always minimum phase.

To illustrate this result, let us consider objects that satisfy the velocity transfer assumption. For these examples, the impedance of the object is generated by the following Fourier series with real-valued Fourier coefficients:

$$z_{vt}(\omega) = a_0 + \sum_{n=1}^{N} a_n \exp\left(\frac{in\pi\omega}{\Omega}\right). \tag{4.23}$$

This function satisfies the causality condition in (2.7) and (2.8), since the Hilbert transform of $\sin(n\pi\omega/\Omega)$ is $\cos(n\pi\omega/\Omega)$. For $n > 0$, the coefficients are chosen by

$$a_n = \frac{a_0(1-2r_n)}{N}, \tag{4.24}$$

where r_n is a random number that is uniformly distributed over the interval $0 \leq r_n \leq 1$. This selection insures that $\Re\{z_{vt}\} > 0$ and the system is therefore passive. In all of our simulations, we set $N = 50$. The leading term, a_0, was used to control the magnitude of the impedance.

In the first example, we set $a_0 = 0.1$ to simulate an approximately pressure-release surface. The real and imaginary parts of the object impedance obtained by using this value in Equations 4.23 and 4.24 are shown in Figure 4.3. The reflection coefficient was evaluated using Equation 4.14. The magnitude and phase of the reflection coefficient are shown in Figure 4.4. In the envisioned applications, the phase would not be known and causality would be used to predict it from the magnitude. To this end, a causally predicted phase computed by inserting the magnitude of the reflection coefficient in (2.20). This phase coincides with the actual phase in Figure 4.4, indicating that the reflection coefficient is indeed minimum phase.

To further illustrate this result, an object with a large reflection coefficient magnitude was simulated by choosing $a_0 = 50$. The real and imaginary parts of the resulting impedance are shown in Figure 4.5, where we see a magnitude that exceeds 0.95 everywhere. The magnitude and phase of the reflection coefficient are shown in Figure 4.6. Again, the causally predicted phase coincides with the actual phase because the reflection coefficient is minimum phase.

4.5 Systems with Perfect Force Transfer

This section describes the minimum phase reflection coefficient that results when an object transmits force perfectly. To achieve this limit, the forces applied to the object by the fluid must be equal but opposite, $F_1 = -F_2$. Physically, this condition results when the mass of the object is small. Newton's second law then requires the net force on the object to be zero. One example of such a system is an air bubble in water.

Applying this condition to Equation 4.11 results in

$$(Z_{11} + Z_{12})V_1 = -(Z_{12} + Z_{22})V_2. \tag{4.25}$$

For this equation to hold for arbitrary frequency-dependent velocities, the impedance matrix must have the form

$$[Z] = \begin{bmatrix} Z_{ft} & -Z_{ft} \\ -Z_{ft} & Z_{ft} \end{bmatrix}, \tag{4.26}$$

where the subscripted ft denotes the assumed "force transfer" property of the object.

Substitution of this result into Equation 4.11 yields the simple relation

$$F_1 = -F_2 = Z_{ft}(V_2 - V_1). \tag{4.27}$$

Recalling that $F_1 = -Z_{fl}V_1$, one finds that this impedance acts in series with the acoustic impedance of the fluid to the left of the piston. Therefore, the normalized effective impedance is

$$z_{eff} = \frac{z_{ft}}{1 + z_{ft}}. \tag{4.28}$$

A schematic of the reduced system is shown in Figure 4.7. This reduced system can also be represented by parallel admittances, so that the effective normalized admittance is $y_{eff} = 1 + y_{ft}$. The reflection coefficient is found from Equation 4.14,

$$R = \frac{1 - y_{eff}}{1 + y_{eff}}. \tag{4.29}$$

It has been shown [21] that the drive-point admittance is also a positive real function. Therefore, its real part is always positive in the lower half of the complex frequency plane and the real part of y_{eff} is always

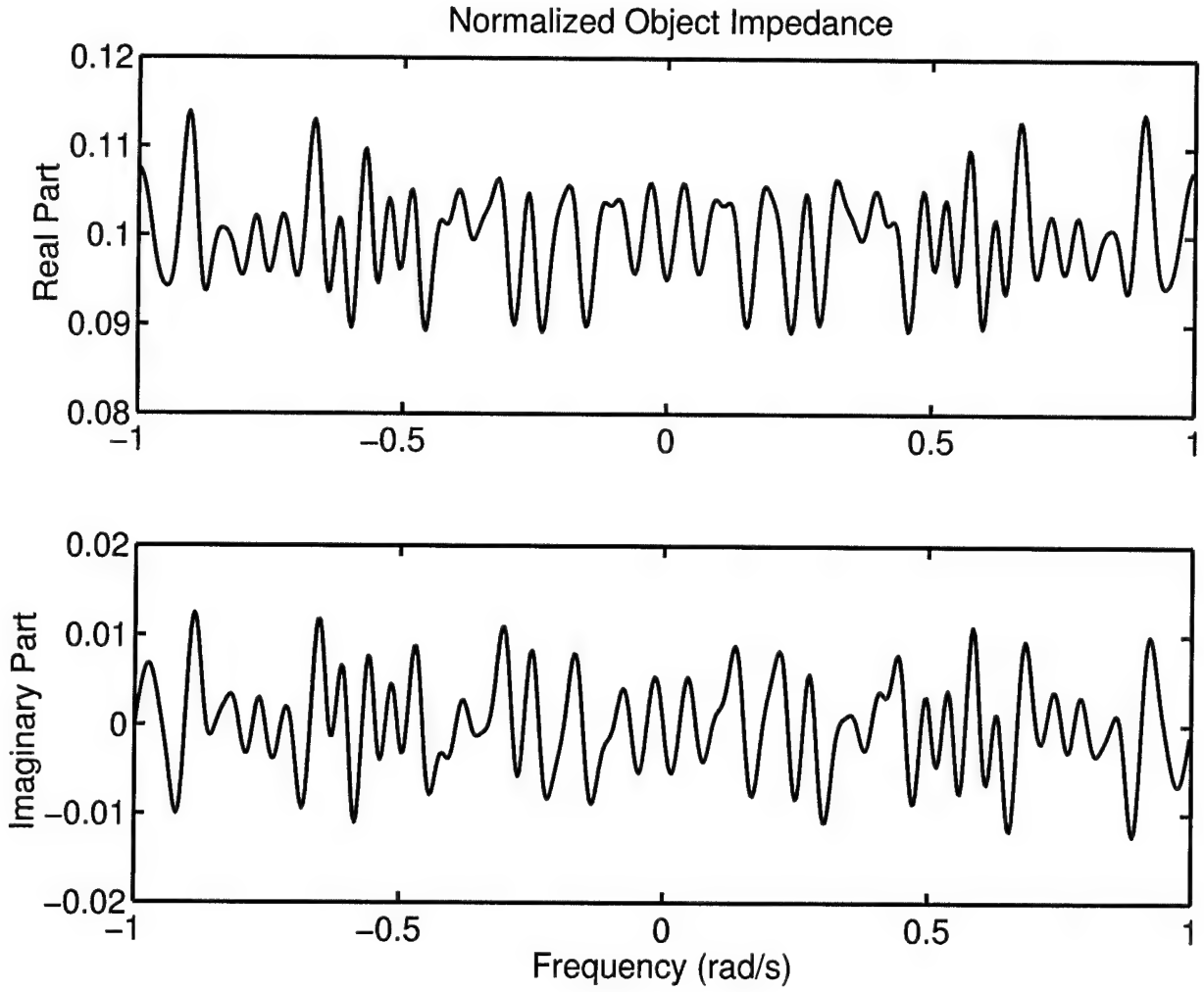

Figure 4.3: Real and imaginary parts of normalized object impedance, z_{vt}, for an object that transfers velocity and has a low magnitude of impedance.

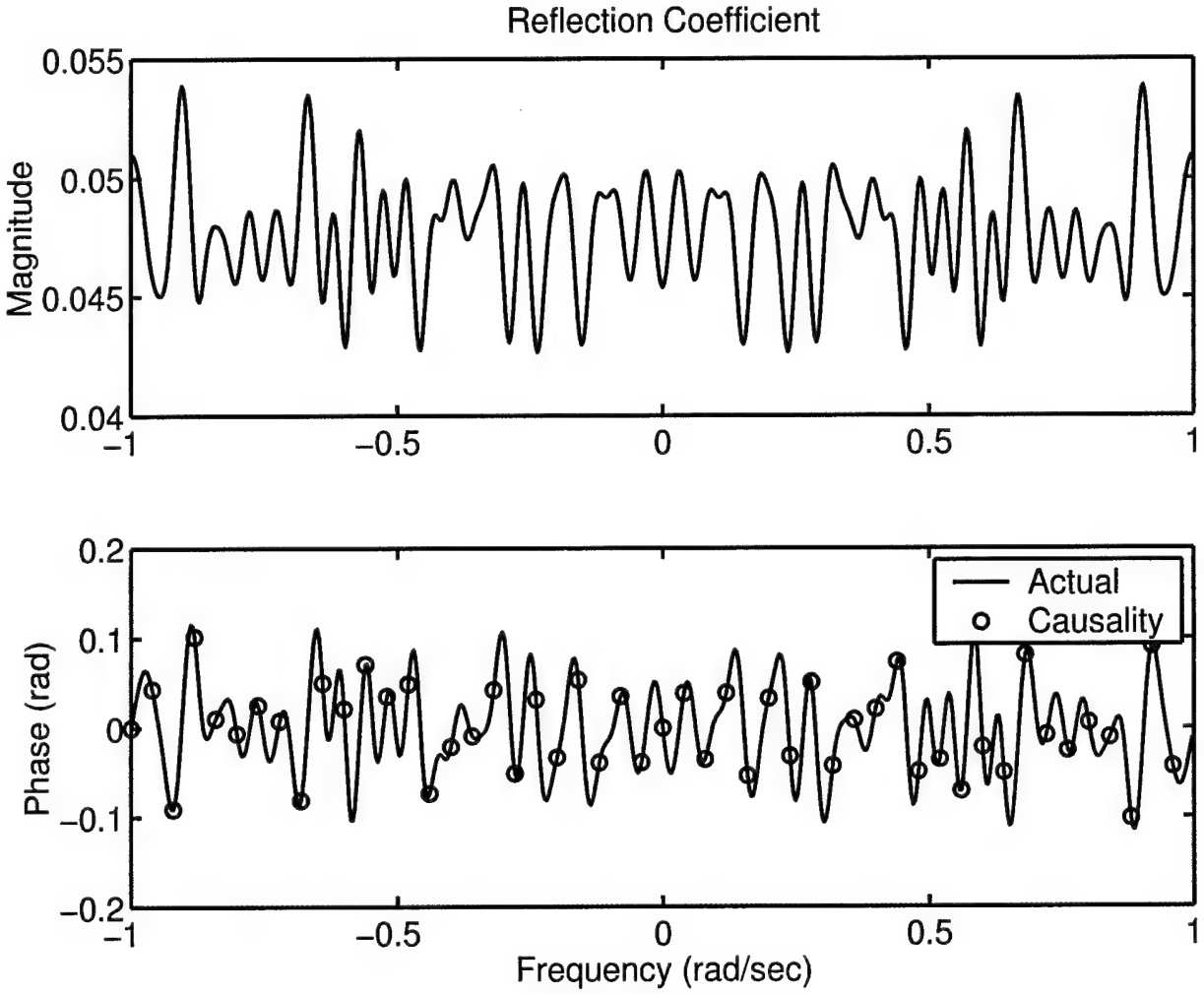

Figure 4.4: Magnitude and phase of the reflection coefficient for an object that transfers velocity and has the impedance shown in Figure 4.3. Causality is used to recover the phase from the magnitude.

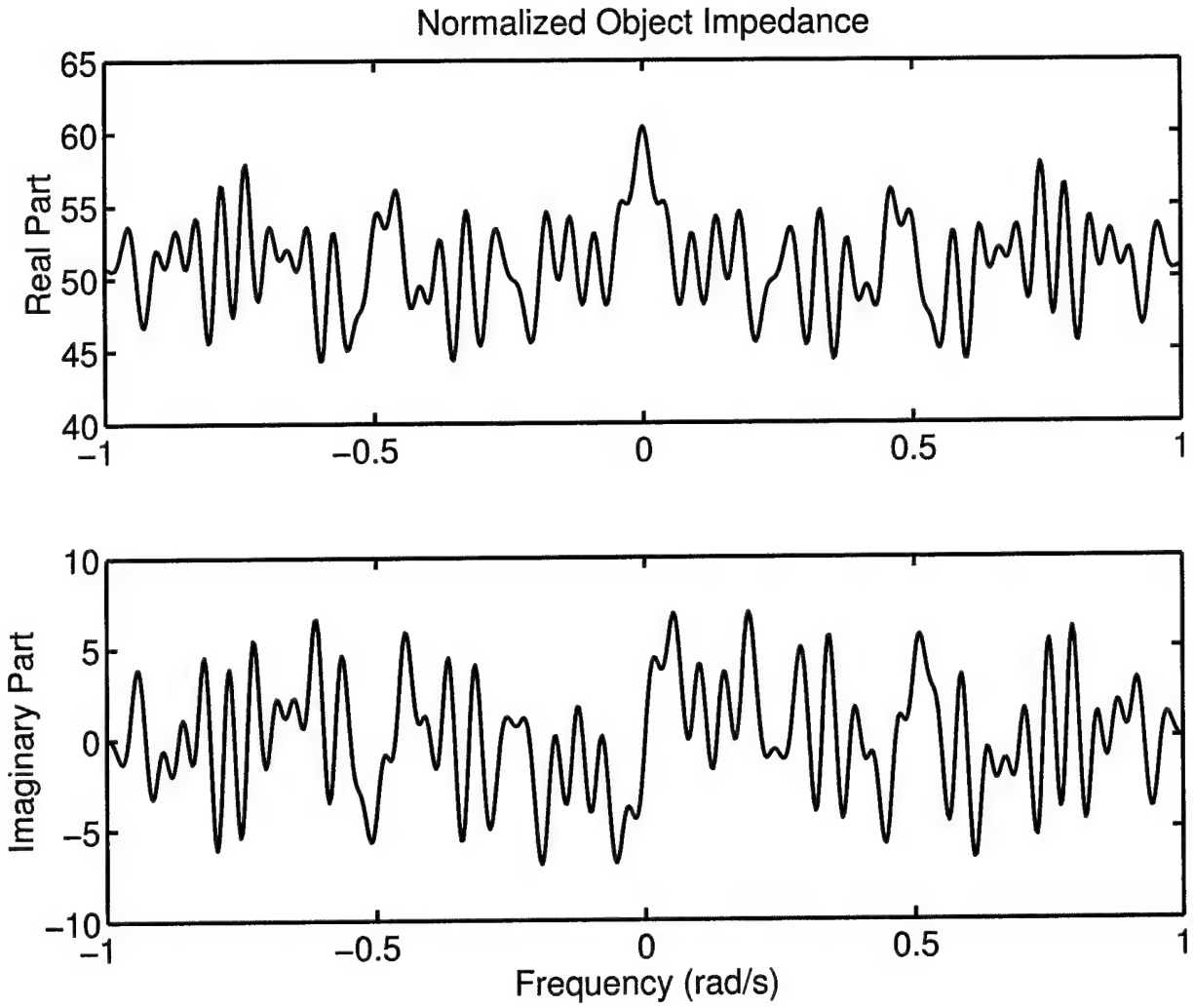

Figure 4.5: Real and imaginary parts of normalized object impedance, z_{vt}, for an object that transfers velocity and has a high magnitude of impedance.

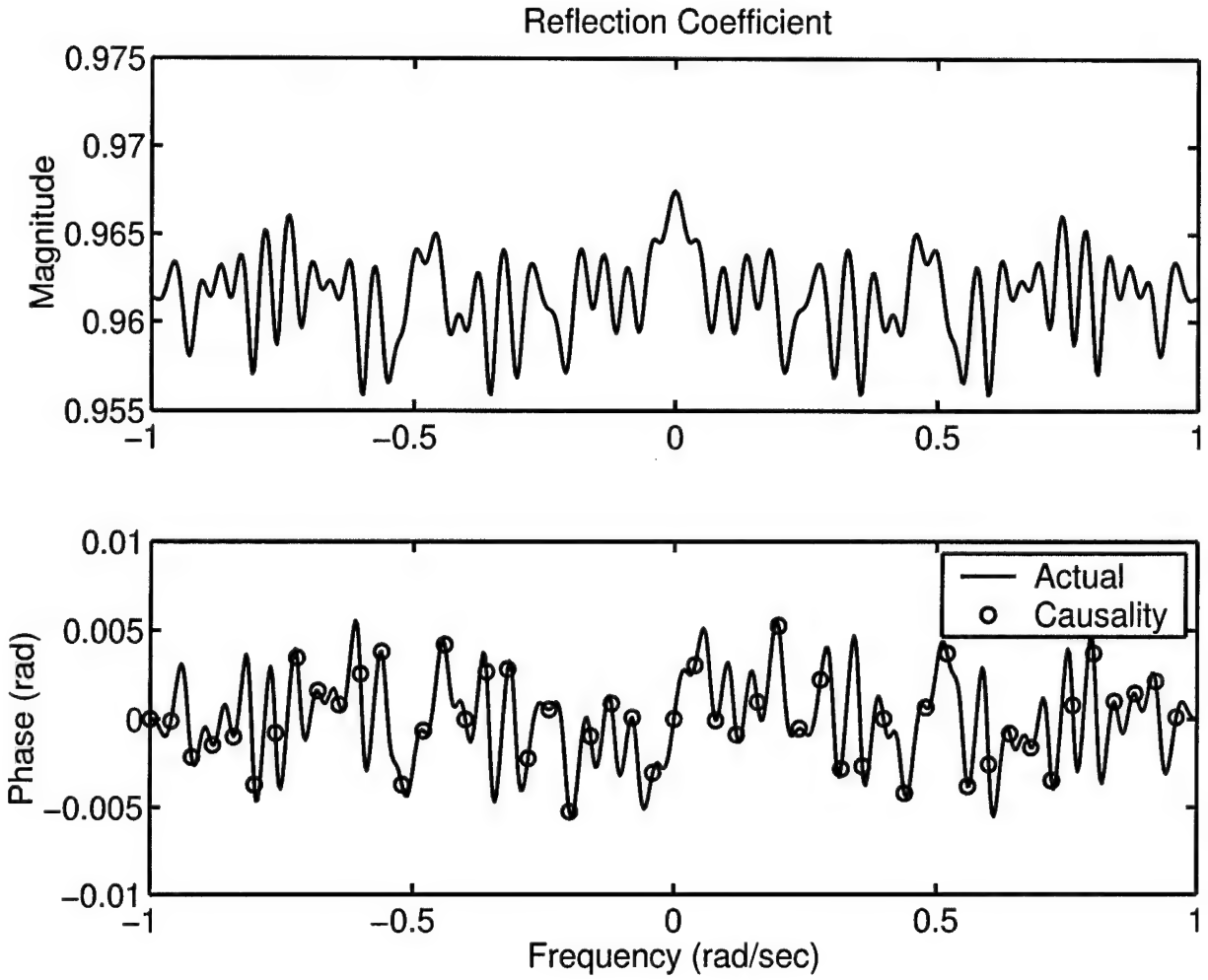

Figure 4.6: Magnitude and phase of the reflection coefficient for an object that transfers velocity and has the impedance shown in Figure 4.5. Causality is used to recover the phase from the magnitude.

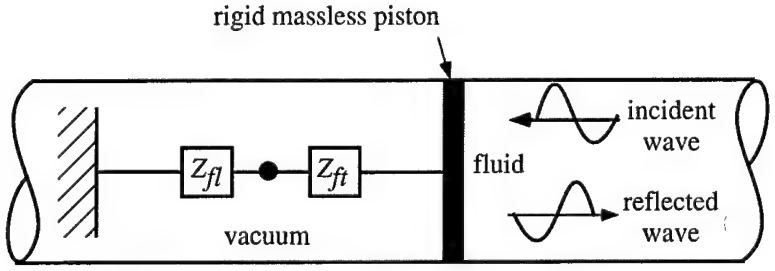

Figure 4.7: A schematic of the system in Figure 4.1 under the assumption that the object transmits force perfectly.

greater than unity. The condition in Equation 4.17 is met and the reflection coefficient is always minimum phase.

This finding will be illustrated by generating random admittances in the same way that random impedances were generated in the previous section. The admittance of the object is generated by the following Fourier series with real-valued Fourier coefficients:

$$y_{ft}(\omega) = a_0 + \sum_{n=1}^{N} a_n \exp\left(\frac{in\pi\omega}{\Omega}\right), \tag{4.30}$$

which is causal and real-valued in the time domain. The passivity condition is satisfied by the choice of a_n given in Equation 4.24. Again, we set $N = 50$ in all of the examples.

Choosing $a_0 = 50$ creates a large object admittance that results in a small reflection. The real and imaginary parts of the object admittance obtained by using this value in Equations 4.30 and 4.24 are shown in Figure 4.8. In order to show that the reflection coefficient for this object is minimum phase, it was evaluated using Equation 4.14. The magnitude and phase of the reflection coefficient computed from Equation 4.29 are shown in Figure 4.9. As in the previous section, a causally predicted phase is computed by inserting the reflection coefficient magnitude in (2.20). This phase coincides with the actual phase in Figure 4.9, indicating that the reflection coefficient is indeed minimum phase.

This finding persists even when the object admittance is very low. Choosing $a_0 = 0.1$ creates a low admittance whose real and imaginary parts are shown in Figure 4.10. Figure 4.11 shows the magnitude and phase of the associated reflection coefficient. Again, the agreement between the actual phase and the causally predicted phase confirms the analytical result that the reflection coefficient is minimum phase.

4.6 Observations

A response-based description of the minimum phase condition in the time domain has been developed and applied to the one-dimensional interactions of acoustic waves with a submerged object. This description decomposes the nonminimum phase reflection into the reflection from an equivalent minimum phase structure and the radiation created by a forcing function applied to the object. An energy-based description of the minimum phase condition presented by Eisner has also been valuable. In particular, this description reveals that an object with a minimum phase reflection coefficient returns energy to the fluid sooner than an equivalent nonminimum phase object.

A condition on the impedance matrix was derived that guarantees a minimum phase reflection coefficient. While the condition is impossible to evaluate in cases where only the reflection coefficient magnitude is measured, it did lead to two special cases. In particular, it was shown that submerged objects that either transmit force or velocity from one body of fluid to another always create minimum phase reflection coefficients. The proofs were based on the positive real properties of drive-point impedance and admittance. The numerical examples confirmed these analytical results for structures with small and large reflection coefficients.

The results of this one-dimensional study are expected to be useful in two contexts. First, the results will be applicable to problems involving acoustic transmission through nonhomogeneous layers that satisfy either the force or velocity transfer condition. Here, the results allow one to characterize the frequency-dependent layer properties by only measuring the magnitude of reflected sound. Second, the results will provide a basis for analyzing more complex three-dimensional scattering problems. For example, monostatic scattering measurements for three-dimensional structures can be modelled by replacing the structure with an effective impedance screen that is perpendicular to the incident wave front. This should be addressed in future work.

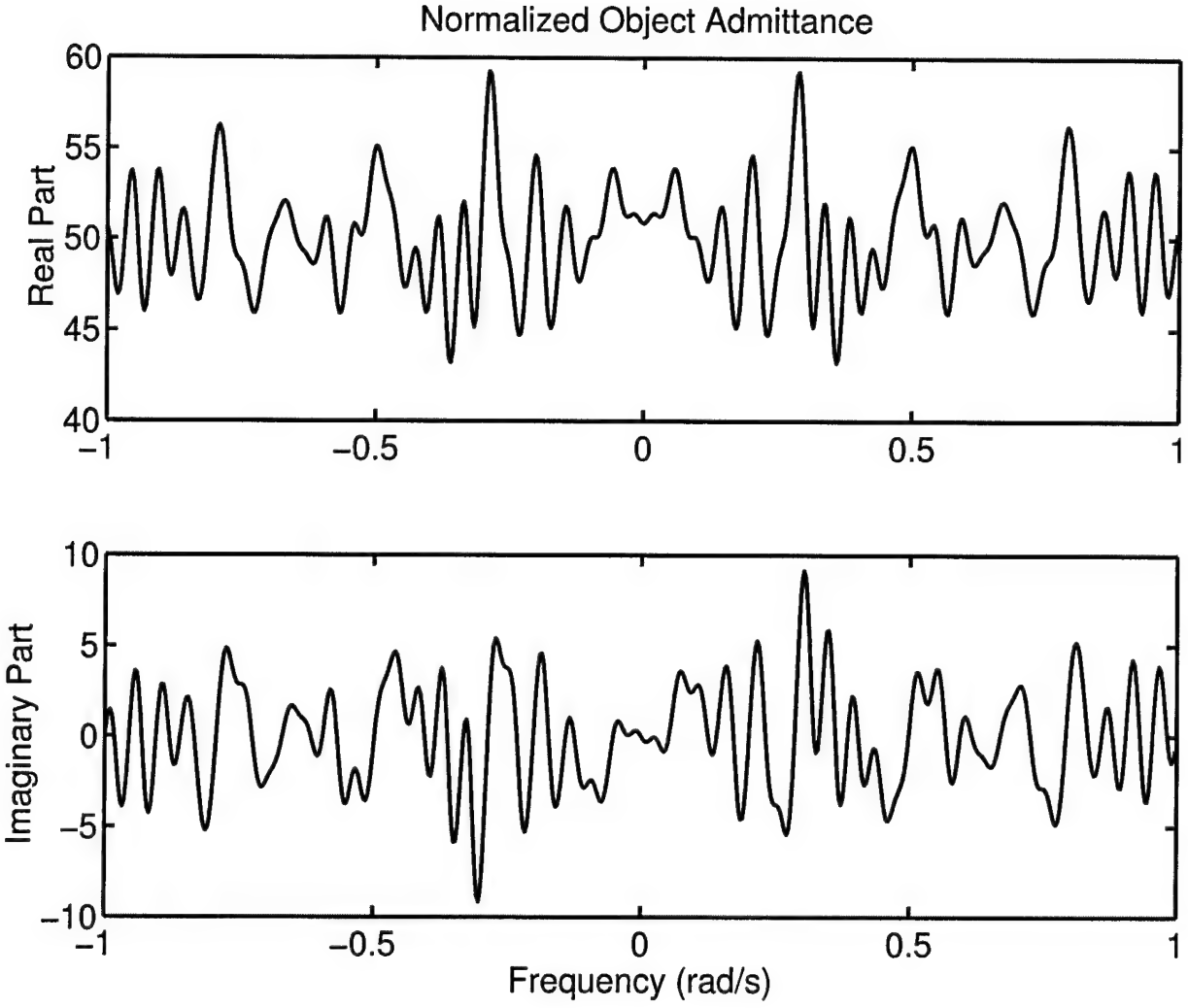

Figure 4.8: Real and imaginary parts of normalized object admittance, y_{ft}, for an object that transfers force and has a high magnitude of admittance.

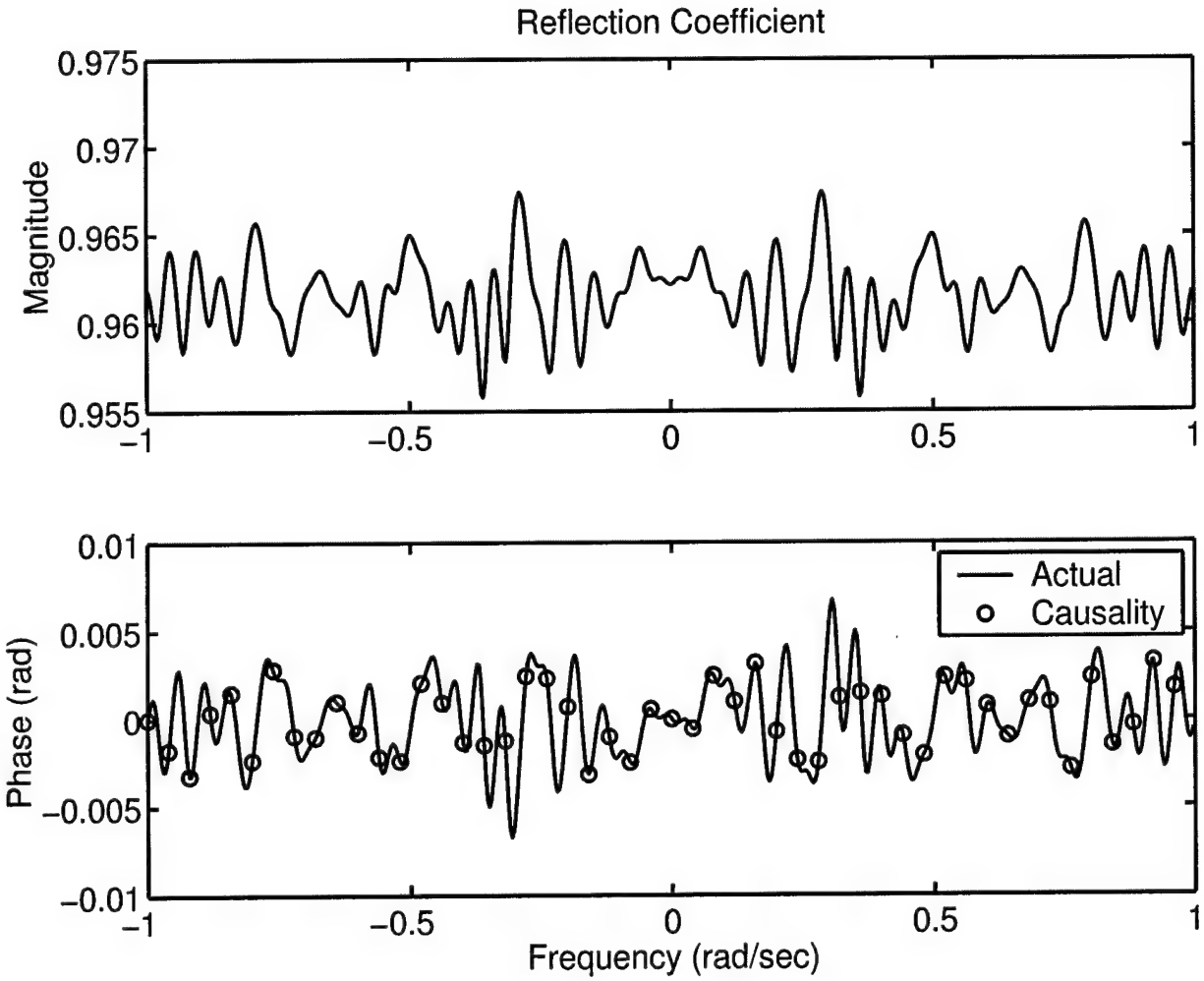

Figure 4.9: Magnitude and phase of the reflection coefficient for an object that transfers force and has the admittance shown in Figure 4.8. Causality is used to recover the phase from the magnitude.

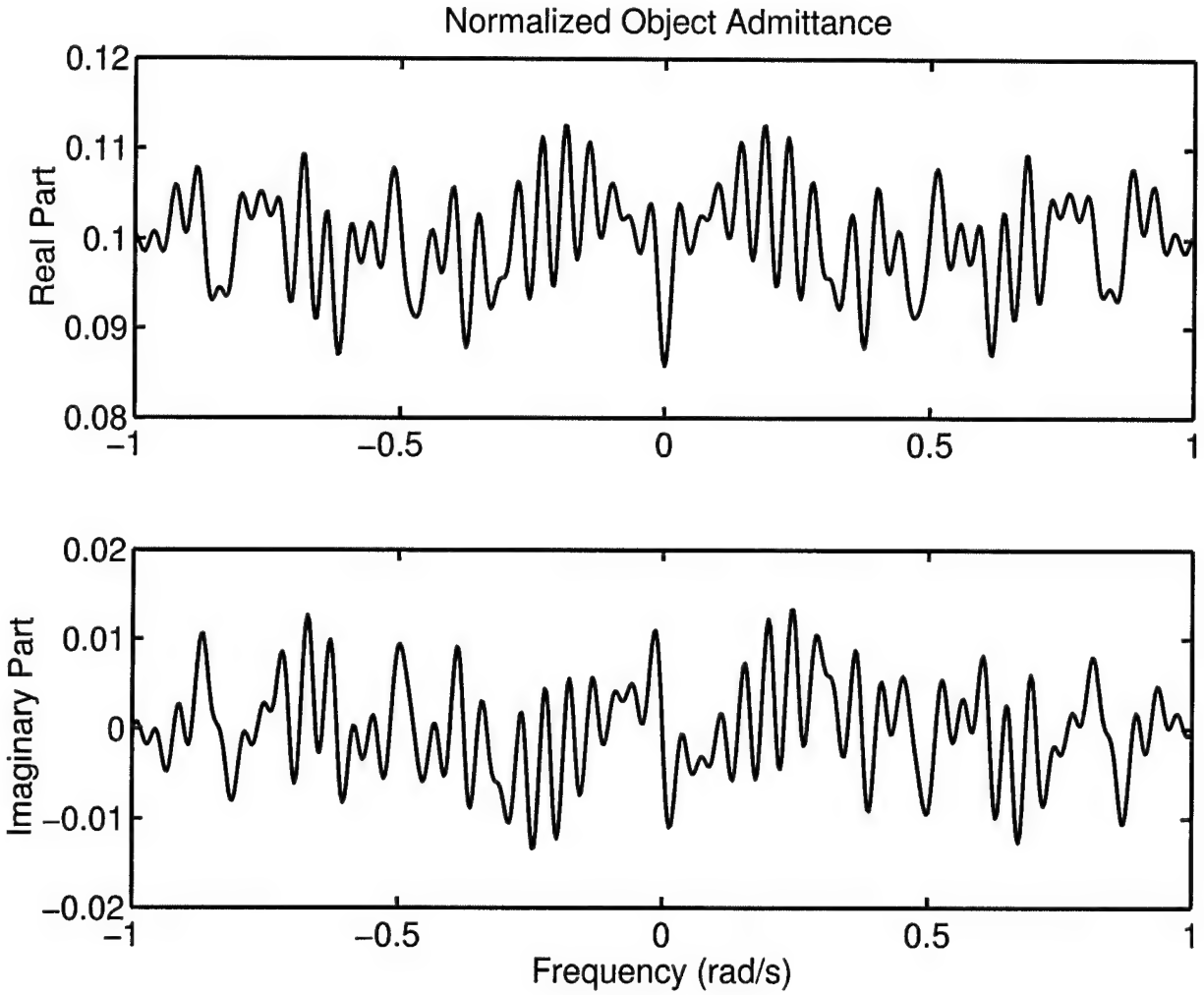

Figure 4.10: Real and imaginary parts of normalized object admittance, y_{ft}, for an object that transfers force and has a low magnitude of admittance.

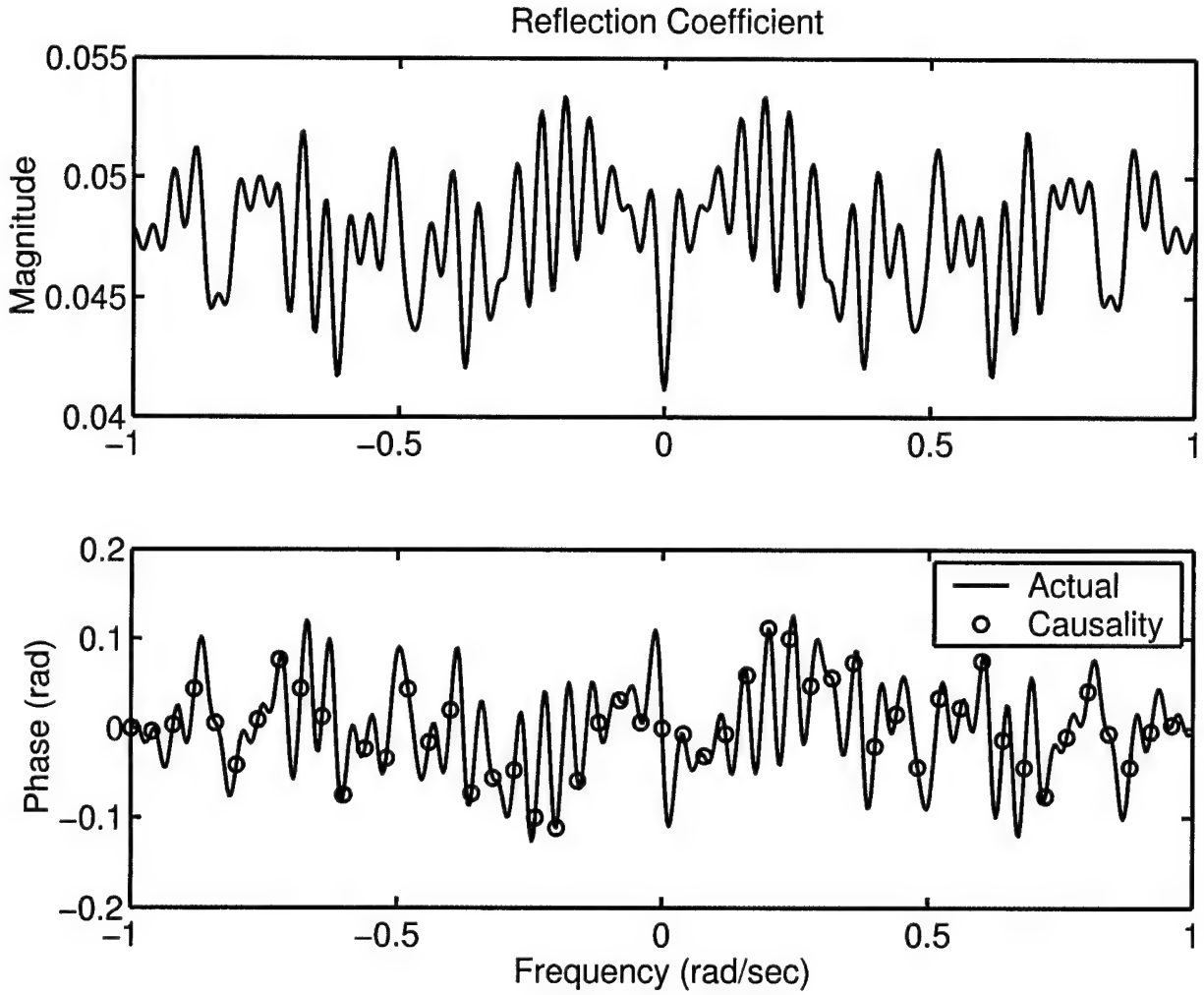

Figure 4.11: Magnitude and phase of the reflection coefficient for an object that transfers force and has the admittance shown in Figure 4.10. Causality is used to recover the phase from the magnitude.

Chapter 5

Causal Removal of Phase Noise

5.1 Introduction

Response data measured as the excitation frequency is varied may be noncausal. For example, consider a one-dimensional acoustic reflection experiment in which the frequency of an incident wave is varied and the reflection is measured at each frequency, giving a complex-valued reflection coefficient. If the location of either the source or receiver is incorrectly measured from frequency to frequency, the phase of the reflection coefficient will be in error and a portion of this error is likely to be noncausal. The magnitude will not be affected. In multidimensional problems, the situation is not so clear but it appears that experimental errors most often affects the phase of the scattered pressure and not the magnitude.

In this chapter, a method is proposed for correcting phase errors with the causality condition and is applied to the one-dimensional reflection experiment. The approach finds the causal reflection coefficient that is closest to the measured noncausal one by a least-squares fit of an implicitly causal expansion to the measured values at each measurement frequency. The accuracy of the method improves when the number of measured frequencies is greater than the number of Fourier harmonics in the data.

5.2 Analytical Formulation

The reflection coefficient is causal because one does not expect a reflected wave until the incident wave strikes, but non necessarily minimum phase. For this reason, the implicitly causal expansion in (3.3) is used,

$$R(\omega) = \sum_{n=0}^{N} r_n \exp\left(\frac{-in\pi\omega}{\Omega}\right) \tag{5.1}$$

This expansion is required to match the experimentally measured reflection coefficient, $\tilde{R}$, at each measured frequency, so

$$\sum_{n=0}^{N} r_n \exp\left(\frac{-in\pi\omega_m}{\Omega}\right) = \tilde{R}(\omega_m) \tag{5.2}$$

for $m = 1, 2, \ldots M$. This results in the matrix equation

$$\mathbf{E}\mathbf{r} = \tilde{\mathbf{R}} \tag{5.3}$$

where the matrix is given by

$$\mathbf{E}_{mp} = \left(\frac{-i(p-1)\pi\omega_m}{\Omega}.\right) \tag{5.4}$$

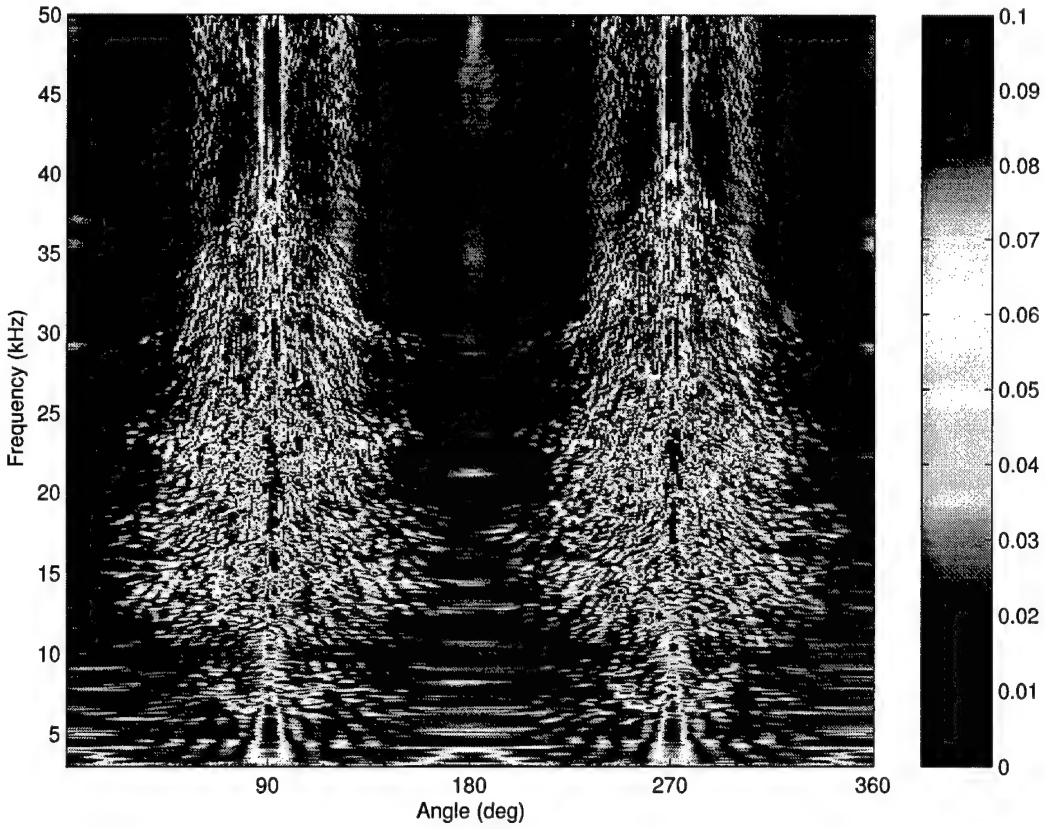

Figure 5.1: Magnitude of the measured reflection coefficient for the NRL experiment.

When $M = (N + 1)$, the system is perfectly constrained and the causal fit will reproduce the measured signal identically. For this approach to be effective, M must be significantly greater than $(N + 1)$. The requirements on M will vary depending on the amount of noise in the data, as illustrated by the examples below. If $M > (N + 1)$, (5.3) is solved in a least squared sense for the Fourier coefficients, which are substituted into (5.1) to recover the reflection coefficient.

The approach contains an interesting self-consistency check which, in our numerical experiments, has been very useful in assessing the accuracy of the method without knowing the answer. If $M > (N + 1)$, the least squares solution of (5.3) does not guarantee that the magnitude of the calculated reflection coefficient will match the measured magnitude. The extent to which this agreement occurs has been an excellent indicator of the accuracy of the recovered phase.

5.3 Application to NRL Scattering Data

The approach was applied to experimental data taken by NRL.[1] The experimental involving multistatic acoustic scattering by a ribbed cylindrical shell with many attached internal oscillators. The farfield acoustic reflection coefficient was measured. Details of the experiment may be found in [23]. The magnitude and phase of the reflection coefficient versus insonification angle and frequency are plotted in Figures 5.1 and 5.2. These plots illustrate the great complexity of structural dynamics that was introduced by the attached oscillators, making this data a significant challenge to the proposed method.

[1]The PI is extremely grateful to NRL for supplying the data, help in using and interpreting the data, and suggestions on this application.

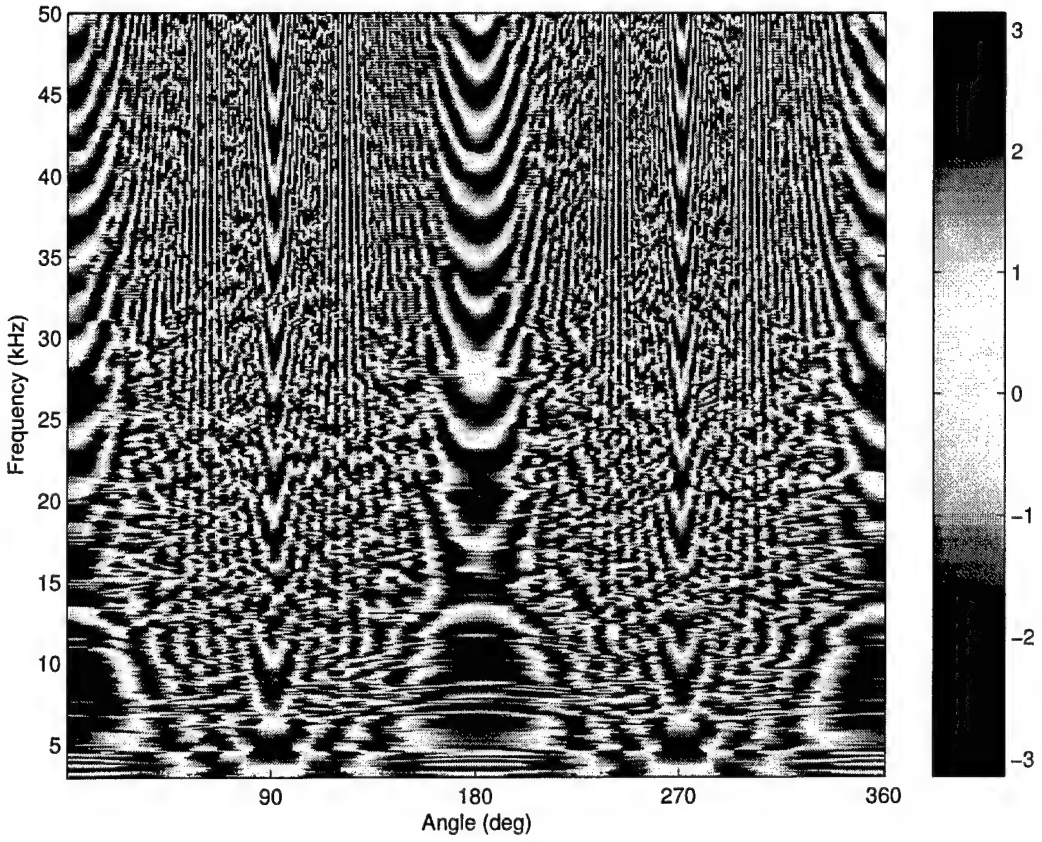

Figure 5.2: Phase of the measured reflection coefficient for the NRL experiment.

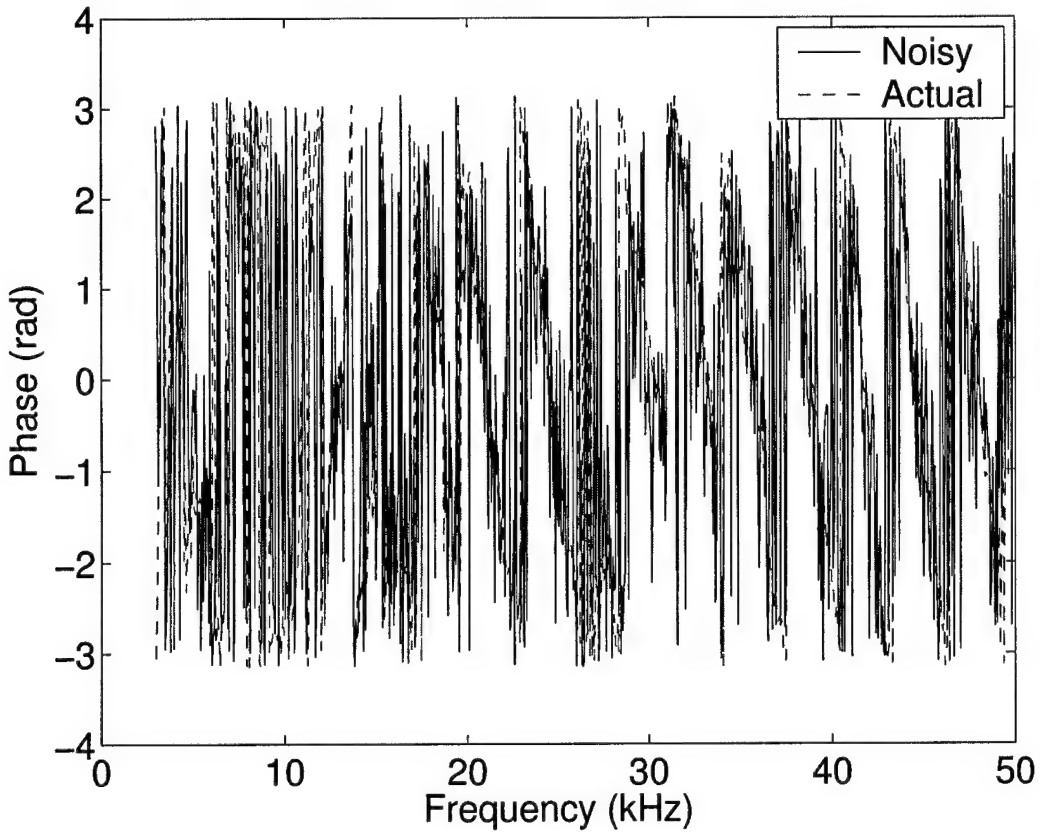

Figure 5.3: Effect of adding noise to the phase of the measured reflection coefficient for the NRL experiment.

Calculations not presented here verified that the measured data satisfied the causality condition to within the numerical accuracy of evaluating the Hilbert transform. Random noise was added to the phase to simulate uncertainties in source or target location. This noise had a normal distribution with a zero mean and 1.5 standard deviation. Figure 5.3 compares the original phase to the simulated noisy phase at the first insonification angle of $\theta = 10^0$. The number of measurement frequencies was $M = 771$ and the truncation in (5.1) was $N = 100$, so that the system of equations in (5.3) was overly constrained. The method recovered phase to the high accuracy shown in Figure 5.4. This same process was repeated for a different insonification angle, $\theta = 120^0$, and these results are shown in Figures 5.5 and 5.6. The accuracy is somewhat less than before, however many gross features of the phase were recovered.

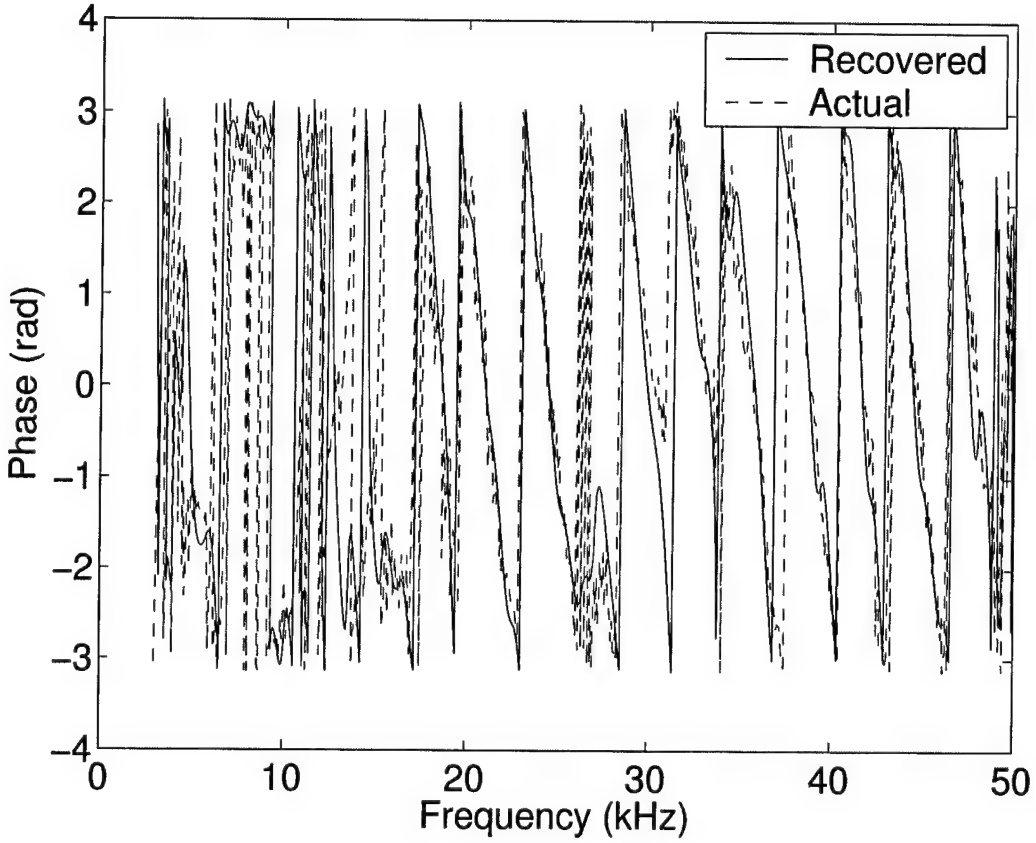

Figure 5.4: Causal removal of noise from the phase of the measured reflection coefficient for the NRL experiment.

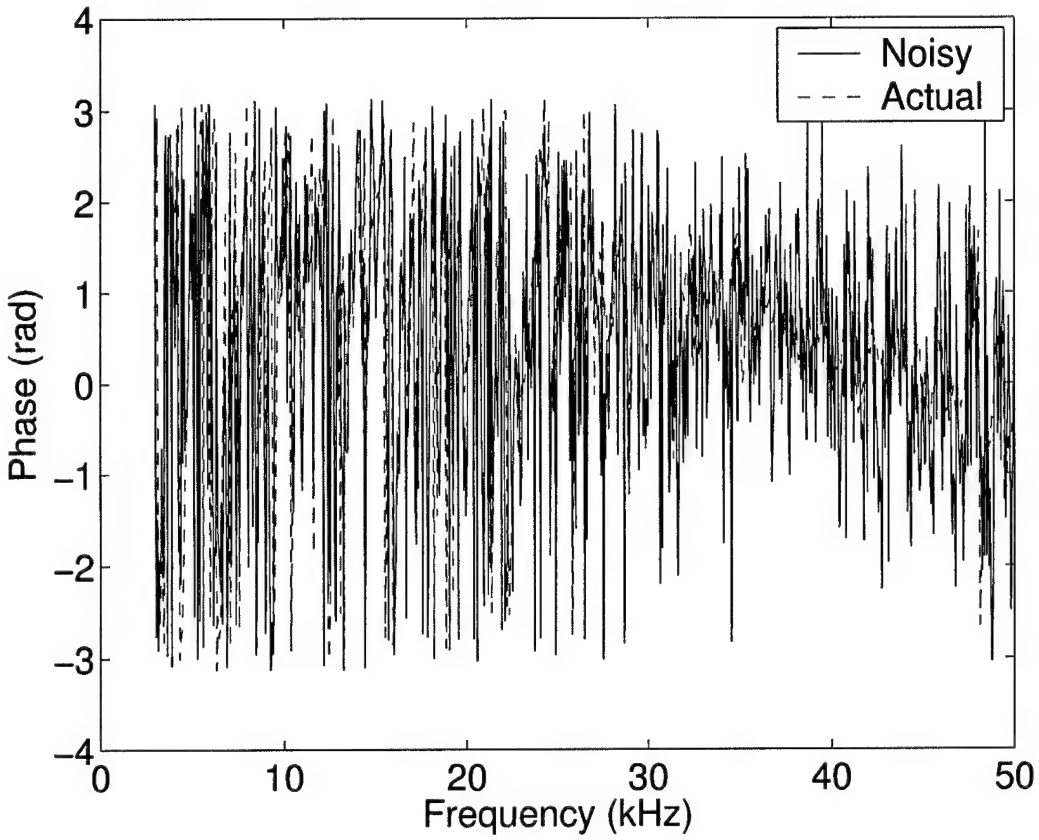

Figure 5.5: Effect of adding noise to the phase of the measured reflection coefficient for the NRL experiment.

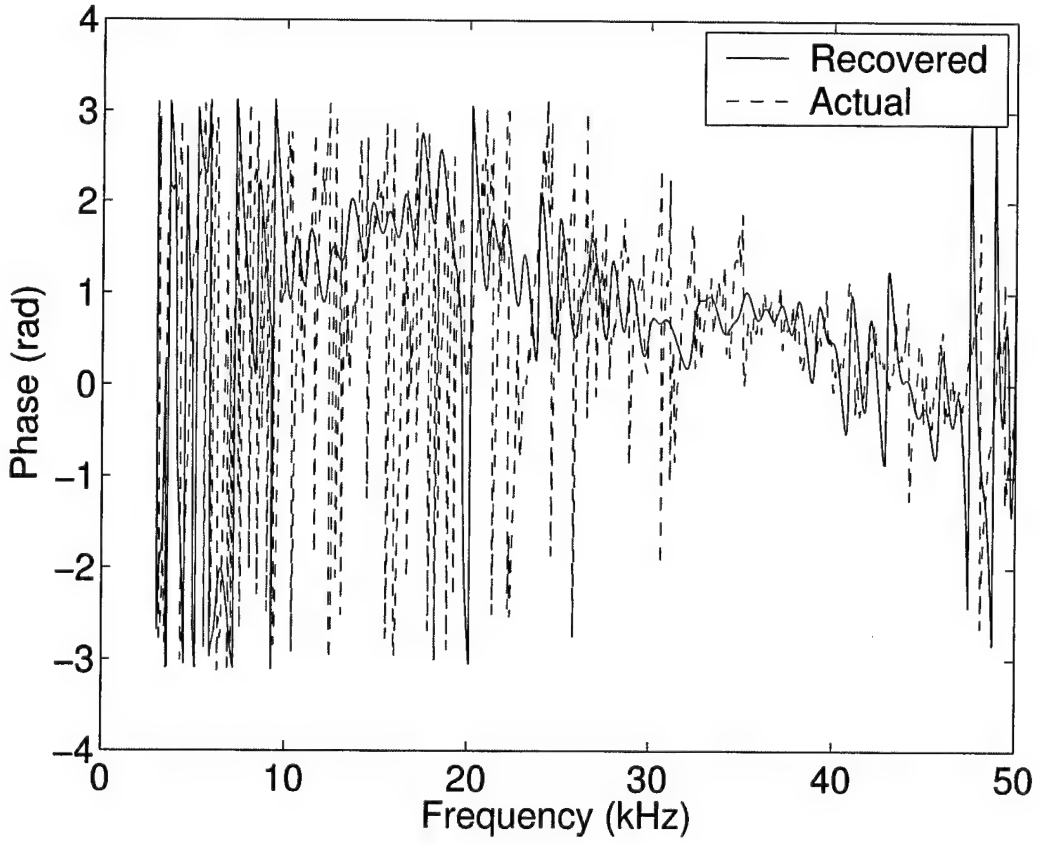

Figure 5.6: Causal removal of noise from the phase of the measured reflection coefficient for the NRL experiment.

Chapter 6

Vibrational and Acoustic Control by Causal Power Absorbers

One means of vibrational and acoustic control is to attach controllers or structures that absorb power, which tends to lower the total energy of the system and globally reduce sound and vibration. This is especially effective in reverberant problems. The approach is described by [24]–[28]. Unfortunately, the absorber that absorbs the maximum amount of power is usually noncausal and can never be physically realized in transient problems. This chapter remedies the situation by finding causal impedances that discretely match the optimal ones in a frequency band. For simplicity, the absorber is assumed here to interact with a two-port system, but the analytical framework presented here will extend to systems with more degrees-of-freedom.

6.1 Analysis of Power Absorption by a Two-Port System

Consider a two-port system with port an excitation at port 1 and an absorber attached at port 2. Linearity leads to equations of motion of the form

$$\left\{ \begin{array}{c} F_1 \\ F_2 \end{array} \right\} = \left[\begin{array}{cc} Z_{11} & Z_{12} \\ Z_{21} & Z_{22} \end{array} \right] \left\{ \begin{array}{c} V_1 \\ V_2 \end{array} \right\} \tag{6.1}$$

where $F_{1,2}$ are forces and $V_{1,2}$ are velocities at ports 1 and 2.

The absorber presents an impedance defined by

$$F_2 = -Z_a V_2 \tag{6.2}$$

Time-averaged power flow to the absorber is

$$P_{out} = \frac{1}{2} \Re \{ -F_2 V_2^* \} \tag{6.3}$$

Combining(6.1), (6.2), and (6.3) relates the power flow to the impedances by

$$P_{out} = \frac{1}{2} |Z_{21}|^2 |V_1|^2 \frac{\Re \{ Z_a \}}{|Z_a + Z_{22}|^2} \tag{6.4}$$

6.2 Absorber Impedance for Maximum Power Absorption

Analysis of (6.4) reveals that the maximum power absorption occurs when

$$Z_a(\omega) = Z_{22}^*(\omega). \tag{6.5}$$

This result is known as *impedance matching* in the electrical literature. One major advantage of maximizing the absorbed power is that it only involves measuring an input impedance and does not require a knowledge of the disturbance. However, the absorber impedance in (6.5) violates the causality conditions in (2.7) and (2.8) for causal structural impedance Z_{22}.

6.3 Causal Impedance for Maximum Power Absorption

Violation of the causality condition for impedance matching is addressed here by expanding the absorber impedance in an implicitly causal and minimum phase Fourier series given in (3.6),

$$Z_a(\omega) = \exp\left[\sum_{n=0}^{N} z_n \exp\left(\frac{-in\pi\omega}{\Omega}\right)\right] \tag{6.6}$$

over the band $\omega_0 \leq \omega \leq (\omega_0 + 2\Omega)$. The Fourier coefficients are required to satisfy (6.5) at selected frequencies ω_m,

$$Z_a(\omega_m) = \exp\left[\sum_{n=0}^{N} z_n \exp\left(\frac{-in\pi\omega_m}{\Omega}\right)\right] = Z_{22}^*(\omega_m), \tag{6.7}$$

where $m = 1, 2, \ldots M$. Taking the logarithm of both sides yields the linear system

$$\mathbf{Ez} = \ln\left(\mathbf{Z}_{\mathbf{22}}^*\right) \tag{6.8}$$

where the matrix is given by

$$(\mathbf{E})_{mp} = \exp\left(\frac{-i(p-1)\pi\omega_m}{\Omega}\right). \tag{6.9}$$

for $p = 1, 2, \ldots (N+1)$.

This system is solved for the vector of Fourier coefficients, $\mathbf{z}$, which is substituted into (6.6) to compute the attachment impedance. The system is perfectly constrained when the number of frequencies is equal to the number of Fourier coefficients, or $M = (N+1)$. In accordance with the discussion in 2.3, the frequencies are chosen over a positive-valued range and the absorber impedance for negative frequencies is found by the conjugate reflection in (2.4) that assures a real-valued impulse response.

6.4 Causal Impedance for Maximum Net Power Absorption

The above approach is very effective for transient disturbances that terminate before energy has an opportunity to interrogate the absorber. In those case, the power input from the disturbance is does not vary with the design of the absorber. For disturbances that do interrogate the absorber, one has the possibility of increasing the power absorbed by increasing the power from the disturbance. Often, the average vibrational power of the system will increase as a result of attaching the absorber. This is usually not desired, as absorbers typically attempt to achieve global control by absorbing power.

We have investigated one solution to this problem that is based on *minimizing the net power into the system* as opposed to maximizing the absorbed power. The absorber impedance that minimizes the net power into the system is also found to be noncausal, however a causal approximation is found using the approach from the previous section.

The analysis begins by formulating the time-averaged net power flow to the two-port system,

$$P_{net} = P_{in} - P_{out} \tag{6.10}$$

where

$$P_{in} = \frac{1}{2}\Re\{F_1 V_1^*\} \tag{6.11}$$

$$P_{out} = \frac{1}{2}\Re\{F_2 V_2^*\} \tag{6.12}$$

$$\tag{6.13}$$

Writing $Z_a = R_a + iX_a$, the absorber impedance that minimizes the net power into the system is found from

$$\frac{P_{net}}{R_a} = \frac{P_{net}}{X_a} = 0. \tag{6.14}$$

Evaluation of these conditions gives a purely imaginary absorber impedance of

$$Z_a = i\left(X_{12}\frac{R_{22}}{R_{12}} - X_{22}\right) \tag{6.15}$$

This impedance essentially reflects the vibrational energy and does not absorb it.

6.5 Numerical Examples

In these examples, drive-point impedances of the 2-port system were generated by randomly choosing 10 Fourier harmonics and constructing them from (3.3). Since passivity requires that a drive point impedance has a positive real part, the phase of the randomly generated transfer functions was scaled to lie between $-0.9(\pi/2) < \theta < 0.9(\pi/2)$. The transfer impedance were generated by taking the reciprocal of admittances generated by randomly choosing 10 Fourier harmonics and and evaluating (3.3). The absorber impedances were found by least squares fits at 10 frequencies and then the expansions were evaluated at 500 frequencies for plotting purposes.

Figure 6.1 shows the real and imaginary parts of an absorber impedance chosen for maximum power absorption. The causal approximation was found by using the expansion in (6.6) with the Fourier coefficients found by evaluating (6.8). At the circled data points, which indicate frequencies at which (6.6) was required to match the optimal impedance, the optimal and causal impedances match. At other points, the impedances differ. The plot of absorbed power in Figure 6.2 shows that introduction of the causality condition reduces the power absorbed, as expected. However, by increasing the number of terms in the Fourier series the causal approximation converges to the optimal transfer function. Note that the causal impedance occasionally becomes active, injecting a net power into the system. This represents a tradeoff in the satisfaction of causality. This process was repeated with the goal of minimizing the net power in, in accordance with the absorber impedance in (6.15). The results are shown in Figures 6.3 and 6.4, where the same observations apply.

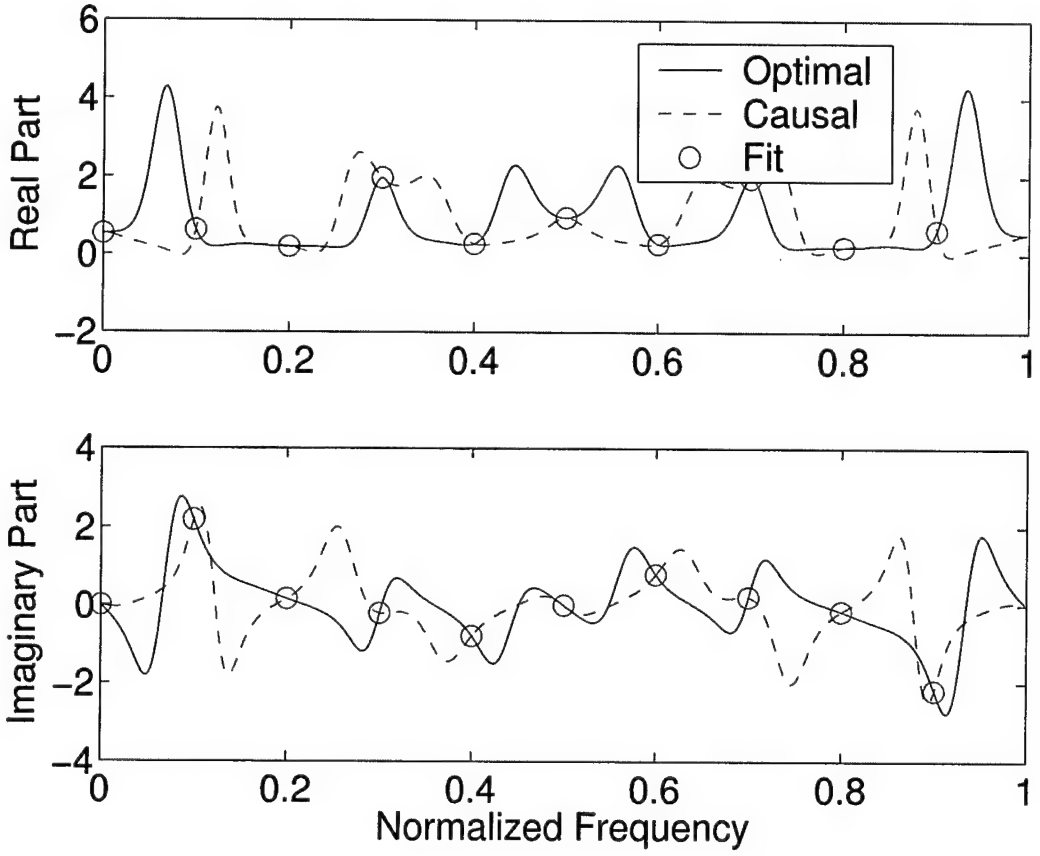

Figure 6.1: Absorber impedances corresponding to optimal but noncausal power absorption and causal power absorption. Circles denote frequencies at which the optimal and causal impedances were constrained to match.

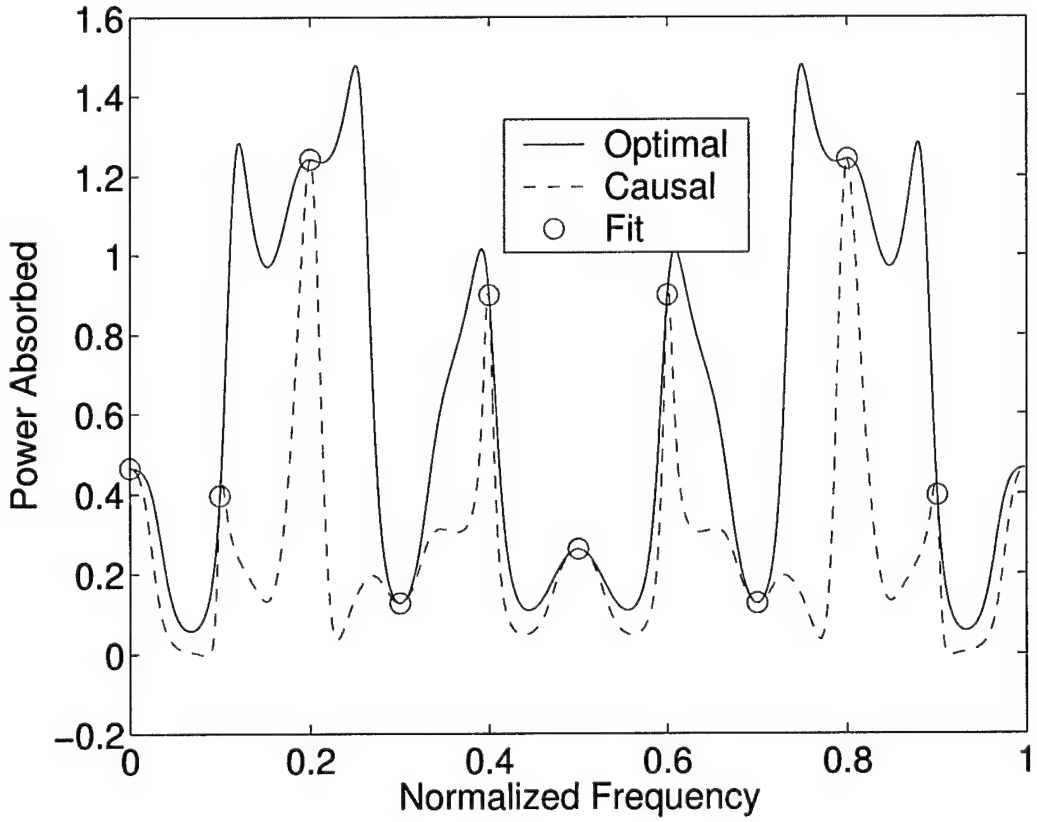

Figure 6.2: Power absorbed by the impedances in Figure 6.1. Circles denote frequencies at which the optimal and causal impedances are constrained to match.

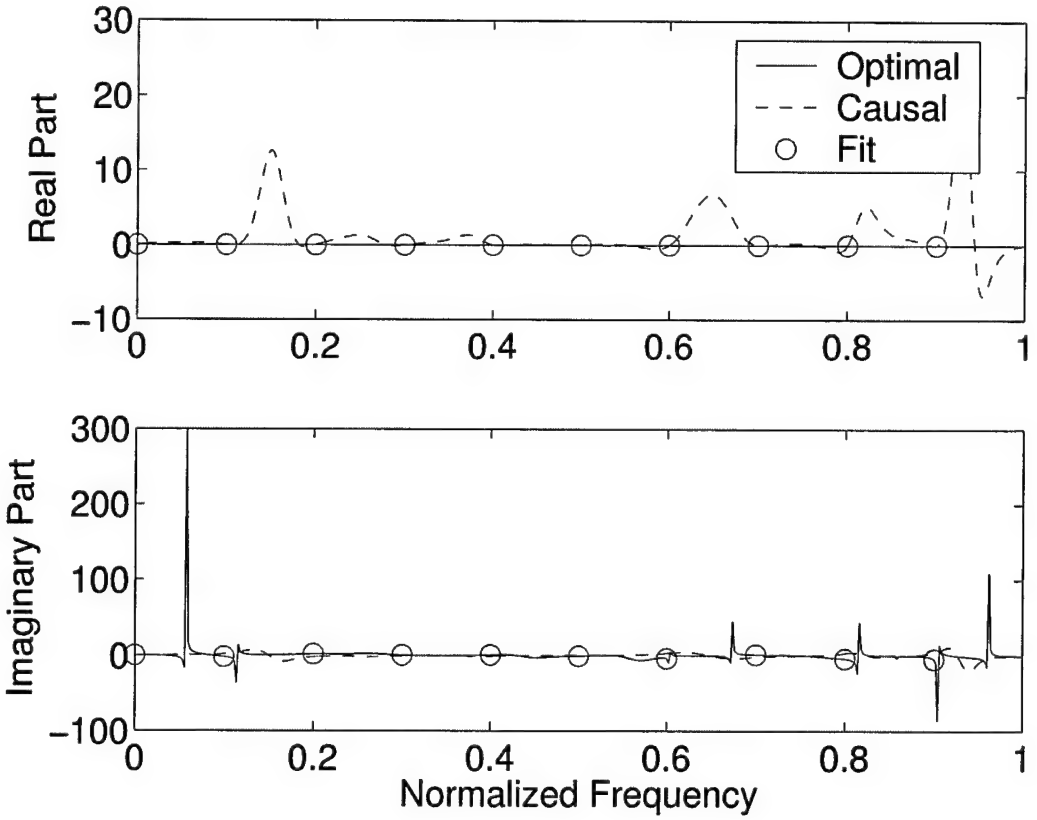

Figure 6.3: Absorber impedances corresponding to optimal but noncausal power absorption and causal power absorption. Circles denote frequencies at which the optimal and causal impedances were constrained to match.

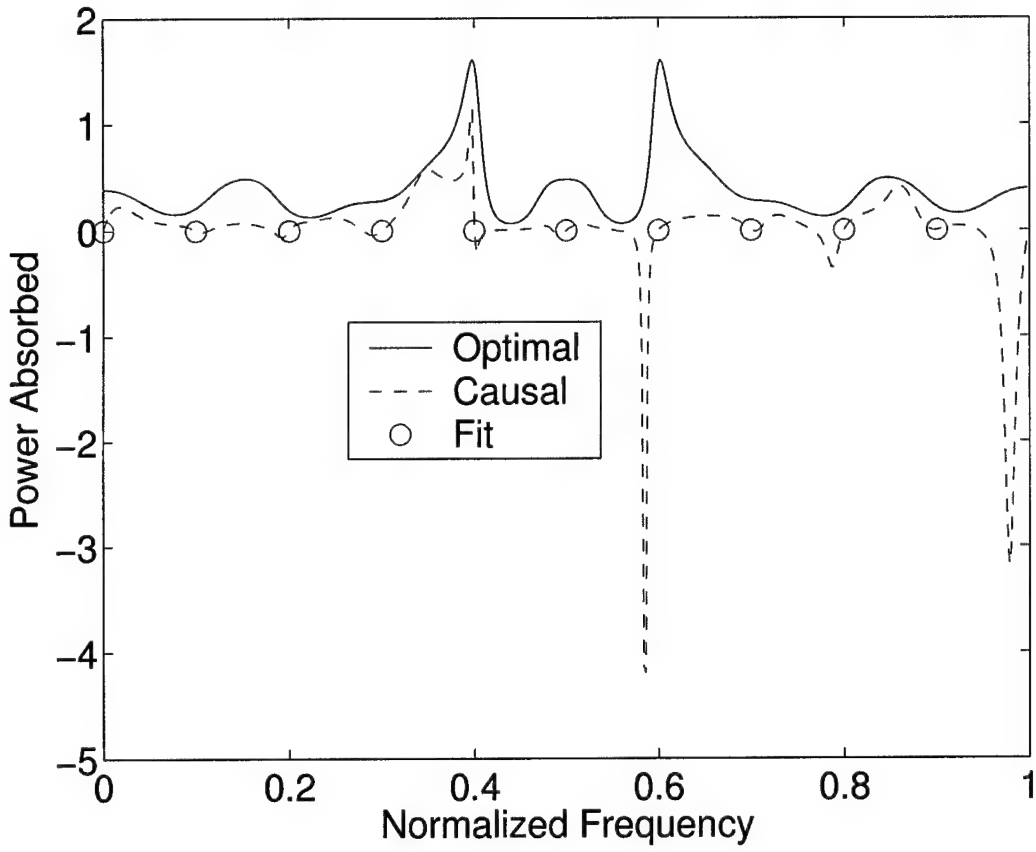

Figure 6.4: Power absorbed by the impedances in Figure 6.3. Circles denote frequencies at which the optimal and causal impedances are constrained to match.

Chapter 7

Causal Interpolation and Extrapolation

7.1 Introduction

In this chapter, a causal reconstruction method for the frequency response of damped structures is developed on the basis of existing sampling theorems. Such reconstructions are useful to understanding the detailed dynamic properties of damped structures. The frequency response should satisfy the causality condition and the real-valued condition when it is taken to the time domain. The reconstruction proposed here is made causal by taking the frequency samples to the time domain, zeroing out the values at negative times, and then returning to the frequency domain. The method guarantees satisfaction of causality condition by eliminating any non-zero values at negative times. An error analysis is carried out and indicates that the accuracy of the method increases with the damping ratio. Numerical examples are used to confirm the analytical findings and to illustrate its capability to reconstruct frequency responses in a frequency range.

The origins of modern sampling theory can be traced back to two persons: Shannon and Kotel'nikov. Shannon's paper [29] has been widely recognized as the first paper on modern sampling theory from the engineering perspective. However, it was later realized that Shannon's result had been discovered in 1933 by a Russian engineer Kotel'nikov [30]. He applied it in communication engineering earlier than Shannon. However, there is no doubt that it was Shannon's paper that triggered a flood of work on this topic, which eventually produced a large body of results on sampling theorems and their applications.

Following their footsteps, Yen [31] derived the minimum norm solution to this problem. It had been recognized for a long time that the minimum-norm solution was ill-conditioned [32]. To correct this, Wingham [33] proposed a singular value decomposition method to provide a series expansion that can identify components of the basis functions that are poorly represented by the sampled data. Soumekh proposed the unified Fourier reconstruction(UFR) method [34], which reconstructs the spatial function by low pass filtering the sampled data. More detailed reviews on the state-of-the-art in sampling theory are given by Unser [35] and Gacia [36].

The sampling theorems have been applied in many branches of science and technology such as, acoustical holography [37], nuclear magnetic resonance imaging [38], and approximation of geophysical potential fields [39]. However, their application to frequency response reconstruction of damped structures has been rare. The reconstruction of frequency response of damped structures has two unique futures that distinguish itself from the other applications. One is that the impulse response in the time domain, which corresponds to the inverse Fourier transform of frequency response should be real-valued. The other is that the impulse response function should be causal, i.e., response is always zero for negative time.

These two distinct features lead to some special requirements that have not are not easily satisfied by existing reconstruction methods. In what follows, two well established reconstruction bases, the trigonometric basis and the sinc bases, are reviewed as background. A new reconstruction basis is presented in section 7.2.

In the derivation, we take the frequency samples to the time domain and zero out the values at negative times. Therefore, the causality condition is implicitly satisfied. Errors generated by the proposed method are analyzed in section 7.3. These errors come from both the time domain truncation and the basis function truncation. Numerical examples in section 7.4.1 show that the proposed method generates smaller errors than existing methods when a causal frequency response from a viscously damped structure is used as a testbed.

7.2 Causal sinc basis

In this section, a new transfer function interpolation basis is derived that satisfies the causality requirement. To reduce the complexity, we assume the samples are evenly spaced. The derivation begins with the following delta function summation describing the sampled pulses as defined by Papoulis [40]

$$H_p(\omega) = \sum_{n=-\infty}^{\infty} H(n\omega_0)\delta(\omega - n\omega_0). \tag{7.1}$$

Taking the inverse Fourier transform of the above equation and using the Poisson sum formula [9] yields

$$h_p(t) = \sum_{n=-\infty}^{\infty} \frac{1}{2\pi} H(n\omega_0)e^{in\omega_0 t} \tag{7.2}$$

$$= T/\pi \sum_{n=-\infty}^{\infty} h(t + 2nT), \tag{7.3}$$

where $T = \pi/\omega_0$ throughout this subsection.

Clearly, (7.3) is a periodic function with period $2T$. If the time domain impulse response $h(t)$ is zero outside $[0, 2T]$, filtering (7.3) with a window function yields the exact impulse response $h(t)$

$$h(t) = \frac{\pi}{T} h_p(t)w(t), \tag{7.4}$$

where the window function is given by

$$w(t) = \begin{cases} 1 & 0 \le t \le 2T \\ 0 & \text{otherwise} \end{cases}. \tag{7.5}$$

Taking the Fourier transform of (7.4) leads to

$$H(\omega) = \frac{\pi}{T} H_p(\omega) * \mathcal{F}\{w(t)\}. \tag{7.6}$$

Substitution of the Fourier transform of $w(t)$

$$\mathcal{F}\{w(t)\} = \frac{2\sin(\omega T)}{\omega} e^{-iT\omega} \tag{7.7}$$

yields

$$H(\omega) = \frac{\pi}{T} \{H_p(\omega)\} * \left\{ \frac{2\sin(\omega T)}{\omega} e^{-iT\omega} \right\}, \tag{7.8}$$

where $*$ denotes convolution.

The definition of the delta function requires that $\delta(\omega - n\omega_0) * F(\omega) = F(\omega - n\omega_0)$. Substituting (7.1) into (7.8) and using this definition gives

$$H(\omega) = 2\pi \sum_{n=-\infty}^{\infty} H(n\omega_0) \cdot S_n(\omega) \cdot E_n(\omega), \tag{7.9}$$

where S_n is given by

$$S_n(\omega) = \frac{\sin(\pi(\omega - n\omega_0)/\omega_0)}{\pi(\omega - n\omega_0)/\omega_0}. \tag{7.10}$$

and $E_n(\omega)$ is given by

$$E_n(\omega) = e^{-iT(\omega - n\omega_0)}. \tag{7.11}$$

Equation (7.9) is a shifted form of Shannon's sampling theorem [9].

The derivation of (7.9) is based on the assumption that the impulse response is zero outside the interval $[0, 2T]$. For a viscously damped structure, the impulse response is not zero beyond $2T$, because it decays to zero only at infinite time. However, as long as T is large enough, or equivalently ω_0 small enough, $h(t)$ can be approximated as zero beyond $2T$, because it decays exponentially. In this case, the transfer function is approximated by

$$H_i(\omega) \approx 2\pi \sum_{n=-\infty}^{\infty} H(n\omega_0) S_n(\omega) E_n(\omega). \tag{7.12}$$

In practical situations, the number of sampled points is limited from $-N$ to N instead of going infinity. Thus the transfer function is further approximated as

$$H_{i,f}(\omega) \approx 2\pi \sum_{n=-N}^{N} H(n\omega_0) S_n(\omega) E_n(\omega). \tag{7.13}$$

It is interesting to note that the new basis functions are combinations of sinc functions and trigonometric functions. The causality condition is implicitly satisfied by (7.13)due to low pass filtering via the window function in (7.5), which eliminates any nonzero values at negative times. To illustrate this, a causal sinc function and its inverse Fourier transform are shown in Figures 7.1 and 7.2. It is clear that the function is shifted by π and the function in time domain is always zero at negative times.

As for the real-valued condition, since the basis functions satisfy $S_{-n}(-\omega) \cdot E_{-n}(-\omega) = S_n^*(\omega) \cdot E_n^*(\omega)$, the inverse Fourier transform of Eq. (7.13) will be real as long as $H(-n\omega) = H^*(n\omega)$.

7.3 Error analysis

The error of the proposed interpolation basis comes from two truncations. One is temporal truncation. The frequency spacing determines T, which is the major filter parameter in the time domain. All values in the time domain beyond $2T$ are truncated. The approximation in going from (7.9) to (7.12) reflects this truncation error. The other truncation is the series truncation. The number of basis functions which is determined by the number of sampled points, is finite instead of infinite. The interpolation basis is truncated at the $(2N+1)$th term, where $(2N+1)$ is the number of samples. The approximation in going from (7.12) to (7.13) reflects this truncation error. The two truncation errors will be discussed separately in this section.

7.3.1 Temporal truncation

To carry out the temporal truncation error analysis, we define two Fourier transform pairs: $h(t)w(t) \leftrightarrow H_1(\omega)$ and $h(t)[1-w(t)] \leftrightarrow H_2(\omega)$ and their interpolation equation H_{1i} and H_{2i}, as in (7.12). Based on the derivation in section 7.2, clearly, $H_{1i} = H_1$. Therefore the temporal truncation error is given by

$$r_1 = |H_i - H| = |H_{2i} - H_2| \leq |H_{2i}| + |H_2| \tag{7.14}$$

$$= |H_{2i}| + \int_{t>2T} |h(t)| dt. \tag{7.15}$$

Transforming $h_i(t) = \frac{\pi}{T} h_p(t) w(t)$ to the frequency domain and using (7.3) yields

$$|H_i| \leq \int_0^{2T} \sum_{n=-\infty}^{\infty} |h(t + 2nT)| dt. \tag{7.16}$$

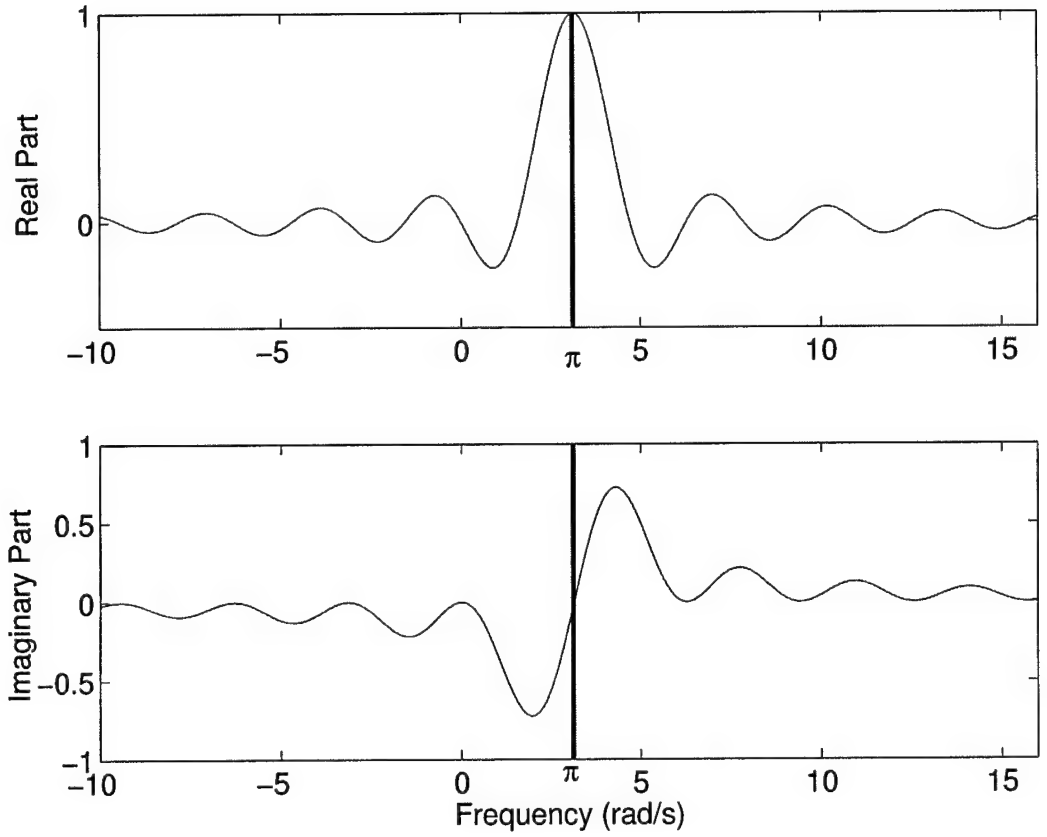

Figure 7.1: Real and imaginary part of a causal sinc function.

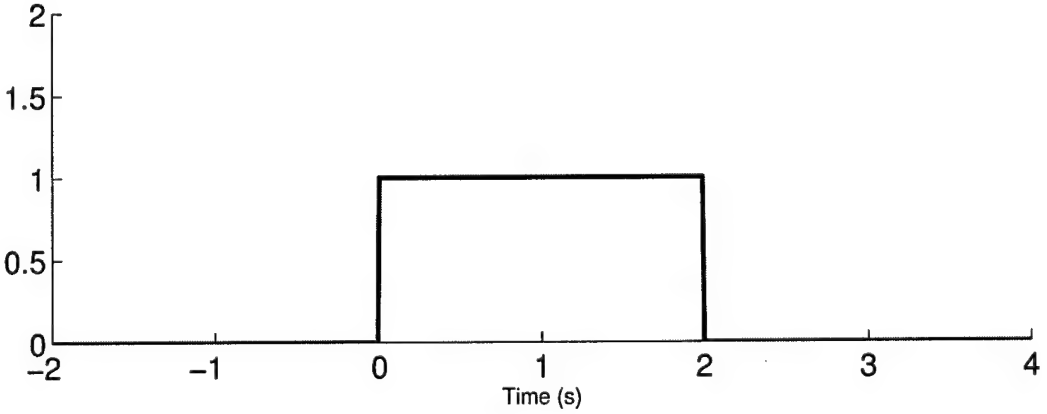

Figure 7.2: Inverse Fourier transform of a causal sinc function.

Interchanging the integral and summation in the above equation gives

$$|H_i| \leq \int_{-\infty}^{\infty} |h(t)|dt. \tag{7.17}$$

Similarly, we have the bound for H_{2i}, which is

$$|H_{2i}| \leq \int_{t>2T} |h(t)|dt. \tag{7.18}$$

Substitution of the inequality (7.18) into (7.15) yields

$$r_1 \leq 2\int_{t>2T} |h(t)|dt. \tag{7.19}$$

7.3.2 Series truncation

If the impulse response only has nonzero values in the interval $[0, 2T]$, its associated frequency response has the important property that

$$|H(\omega)| \leq \sqrt{\frac{T}{\pi}\int_{-\infty}^{\infty} |H(\omega)|^2 d\omega}. \tag{7.20}$$

Here we give a short proof of (7.20). If the impulse response is zero outside the interval $[0, 2T]$, $H(\omega)$ can be written as

$$|H(\omega)|^2 = \left|\int_0^{2T} h(t)e^{-i\omega t}dt\right|^2 \tag{7.21}$$

Considering Schwarz's inequality generates

$$|H(\omega)|^2 \leq \int_0^{2T} |h(t)|^2 dt \int_0^{2T} |e^{-i\omega t}|^2 dt. \tag{7.22}$$

It can be further simplified to

$$|H(\omega)|^2 \leq 2T\int_0^{2T} |h(t)|^2 dt. \tag{7.23}$$

If Parseval's formula is applied to the above equation, (7.20) results.

As has been mentioned before, the series truncation is due to the approximation in going from (7.12) to (7.13). Therefore the error is given as

$$r_2 = |H_i - H_{i,f}|. \tag{7.24}$$

If the function $(H_i - H_{i,f})$ is taken back to time domain, the temporal function will be zero valued outside $[0, 2T]$, because the temporal function is filtered by the window function in (7.5). Applying the property described in (7.20) leads to

$$r_2 \leq \sqrt{\frac{T}{\pi}\int_{-\infty}^{\infty} |H_i - H_{i,f}|^2 d\omega}. \tag{7.25}$$

Combination of (7.12) and (7.13) with the above equation generates

$$r_2 \leq \sqrt{2T\int_{-\infty}^{\infty} |\sum_{|n|>N} H(n\omega_0)\varphi_n(\omega)|^2 d\omega}, \tag{7.26}$$

where

$$\varphi_n(\omega) = S_n(\omega)E_n(\omega) \tag{7.27}$$

The total error due to transfer function interpolation includes contributions from both r_1 and r_2. This error analysis shows that a smaller ω_0 leads to a larger T, which consequently reduces the error contribution from r_1. Or, if the system has a higher damping ratio, the impulse response function $h(t)$ will be smaller outside $[0, 2T]$. The error from r_1 will also be reduced. For the same reason, r_1 will go to infinity if the system has no damping. This predicts that the proposed causal sinc basis does not work for undamped frequency response.

7.4 Applications of the causal sinc basis

The objective of this section is to provide a better understanding of the properties of the causal sinc basis set through some illustrative examples. Two examples are presented. The first example uses mass-spring-dashpot systems to compare the numerical accuracies among the trigonometric basis, Shannon's basis, and the proposed causal sinc basis. The second example uses a numerical model of a realistic engineering structure from the Harwell-Boeing matrix collection. We use different sampling rates to illustrate the performance of the causal sinc basis.

7.4.1 Single degree-of-freedom example

Here we compare the causal sinc basis proposed in section 7.2 with the existing trigonometric basis and the sinc function basis by using two simple examples. First, we examine a single spring-mass-dashpot structure. The system's mass is 1 kg and spring constant is 1 N/m. The damping ratio ζ is equal to 0.2. The exact transfer function is calculated and plotted in Fig. 7.3. The function is sampled with a frequency spacing of 0.16 rad/s within the frequency interval $[0, 2]$ rad/s, and the interpolation is carried out using the three different basis functions. Relative errors for the causal sinc and sinc bases are plotted in Fig. 7.4. The relative error is determined by the ratio of error norm versus the norm of the true value. The comparison between causal sinc basis and trigonometric basis is plotted in Fig. 7.5. The interpolations all tend to have larger error at the boundary region, and the causal sinc basis does not have clear advantage over the others near the boundary. However, it is more accurate than the other two near the resonance frequency. If one is more interested in response values at resonance frequencies, the proposed causal sinc basis would be considered preferable.

We expect the observations from Figures 7.4 and 7.5 to extend to multiple DOFs systems. Here we examine another spring-mass-dashpot problem with three DOFs. The system has undamped natural frequencies at 1, 2, and 3 rad/s with a modal damping ratio of 0.2 at each mode. Figure 7.6 shows the exact transfer function. The response function is sampled at the distance of 0.2 rad/s within the frequency interval $[0, 4]$ rad/s. The interpolation results from the three different bases are compared in Figures 7.7 and 7.8. Once again, the causal sinc basis is more accurate than the other two.

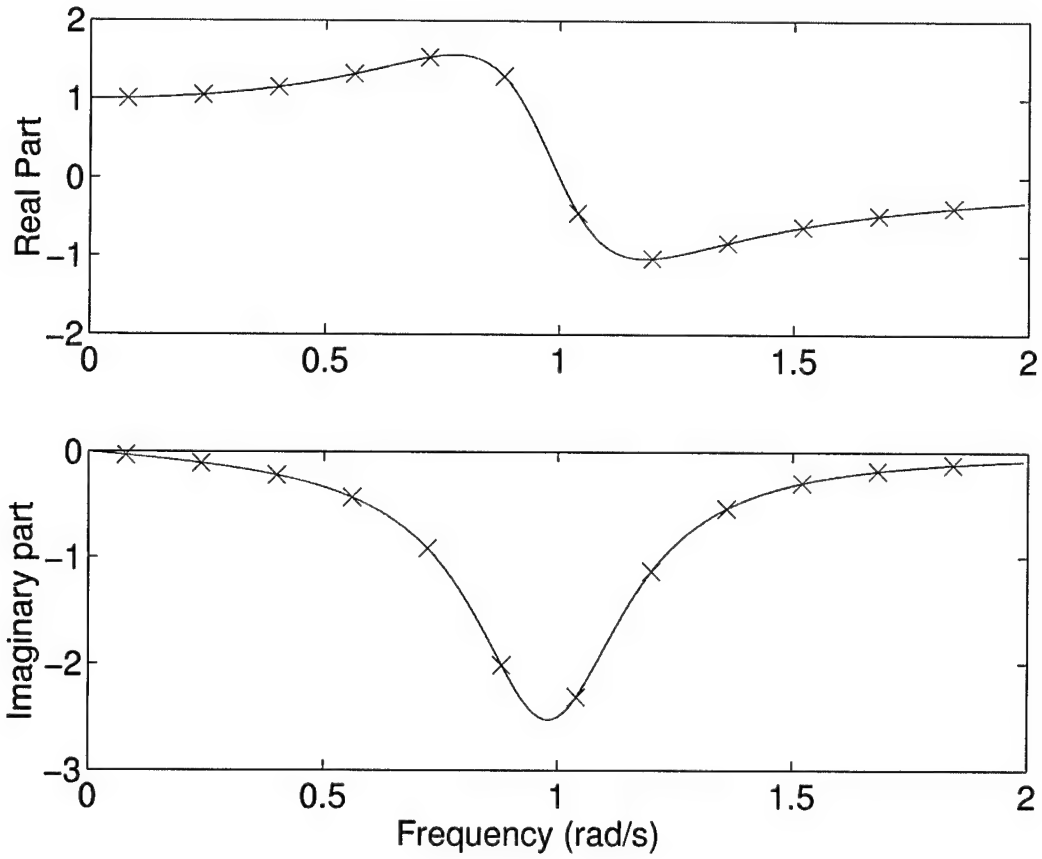

Figure 7.3: Plot of a transfer function for a single spring-mass-dashpot system.

In the error analysis section, we found that the accuracy of the method increases with the damping ratio. We illustrate this conclusion by changing the damping ratio of the single spring-mass-dashpot system and computing the root mean square error for each interpolation. The result in Figure 7.9 supports these analytical results. It also shows that the error will increase around the neighborhood of zero damping, which means the three methods tend to fail when damping approaches zero.

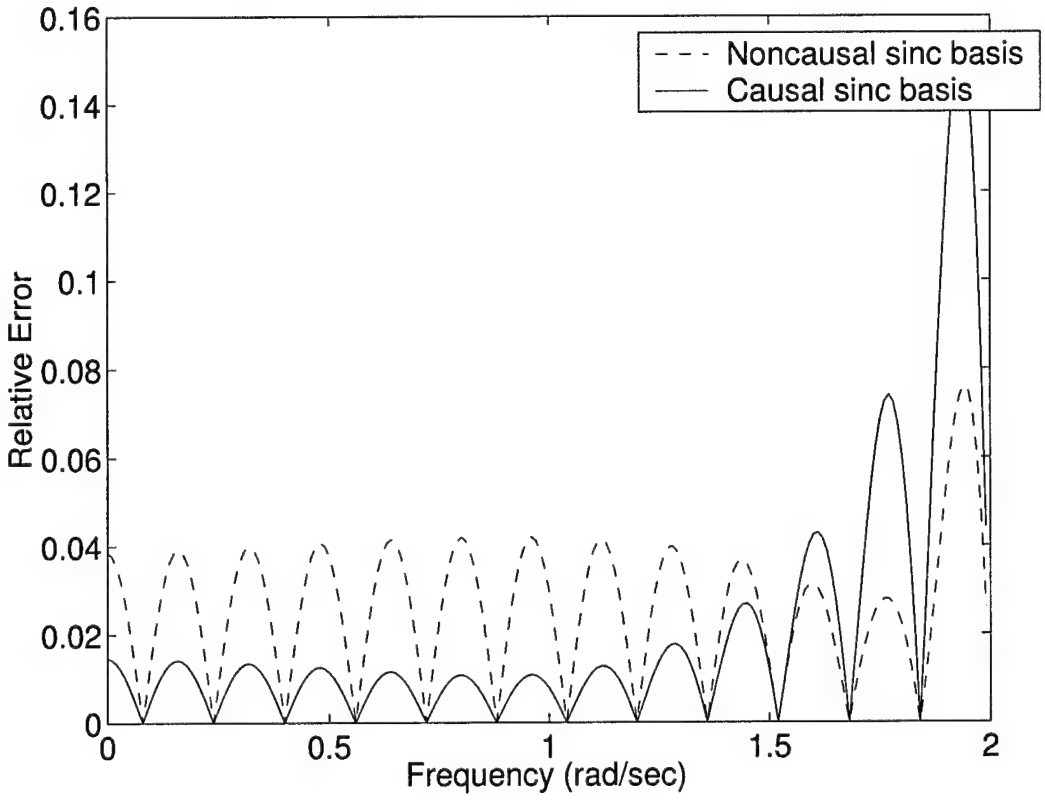

Figure 7.4: Relative errors for the causal sinc and the noncausal sinc bases for the single spring-mass-dashpot system.

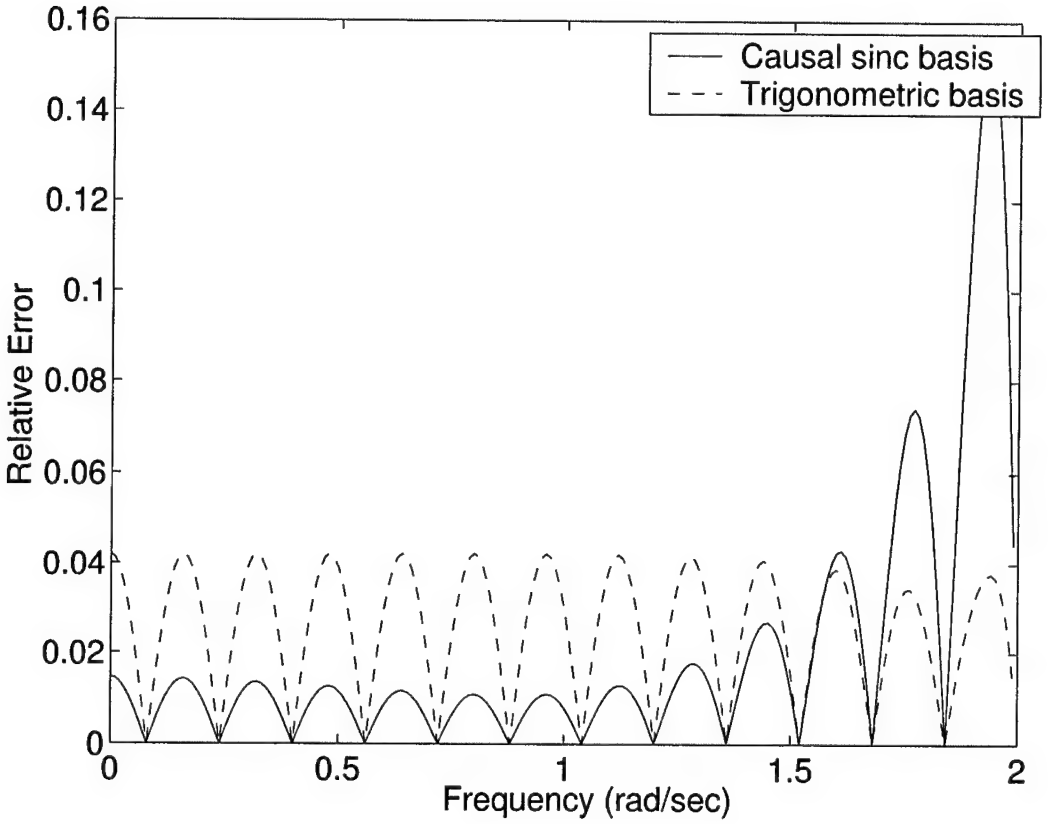

Figure 7.5: Relative errors for the causal sinc and causal trigonometric bases for the single spring-mass-dashpot system.

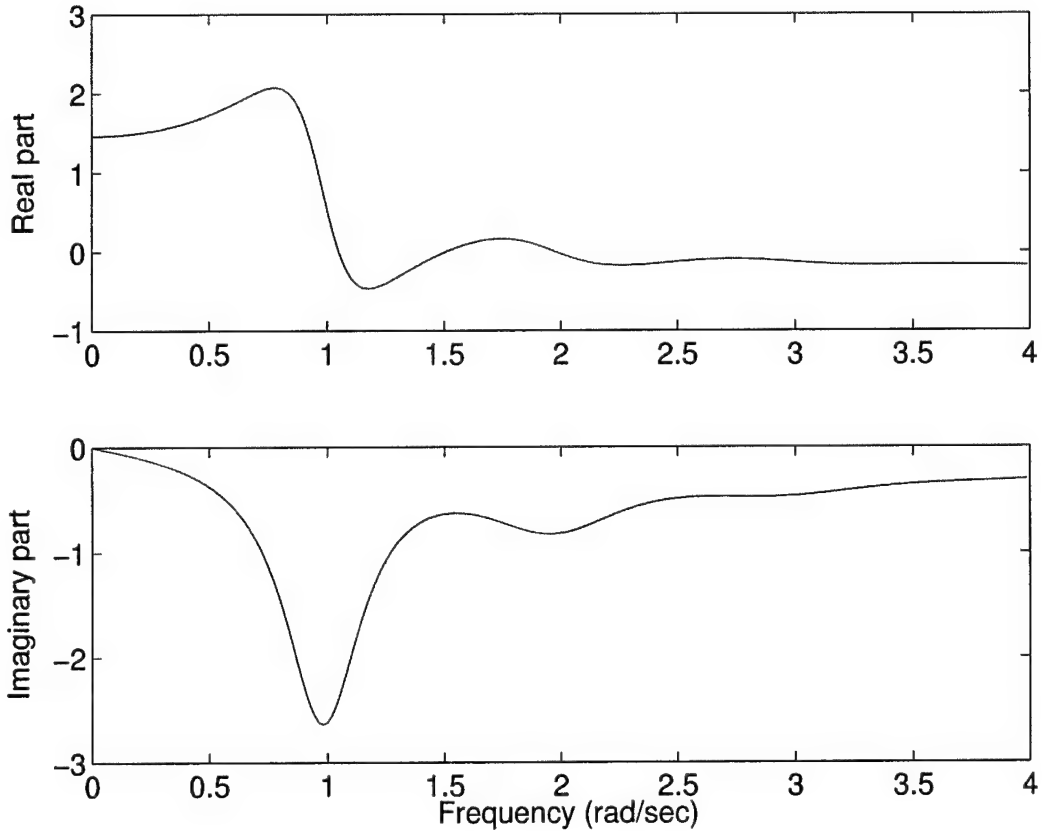

Figure 7.6: Plot of a transfer function for a three DOF system.

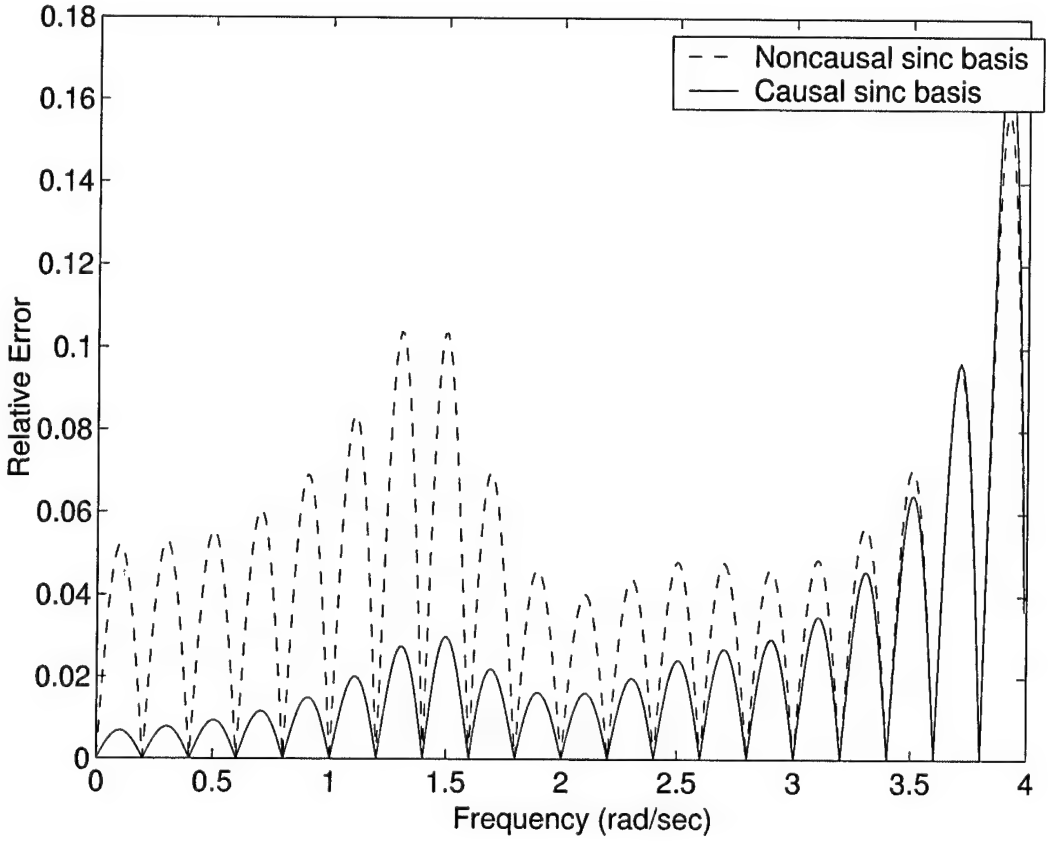

Figure 7.7: Error comparison between causal and noncausal sinc bases for the three DOF system.

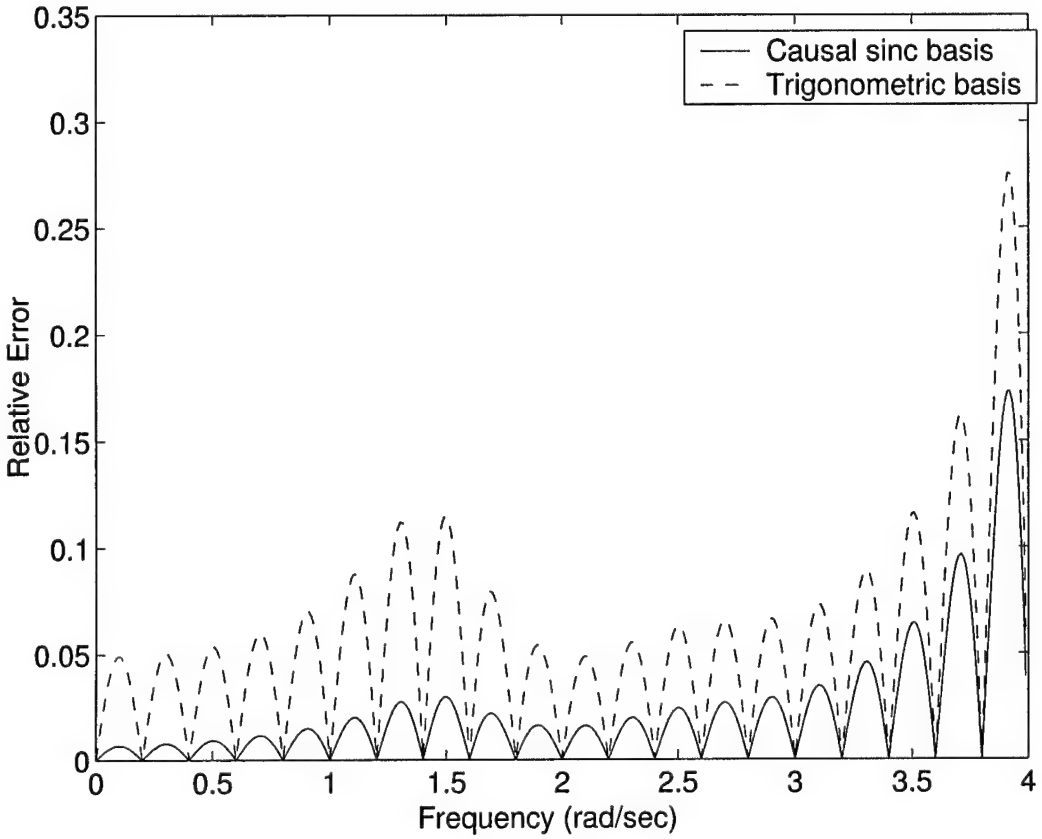

Figure 7.8: Error comparison between causal sinc and noncausal sinc bases for the three DOF system.

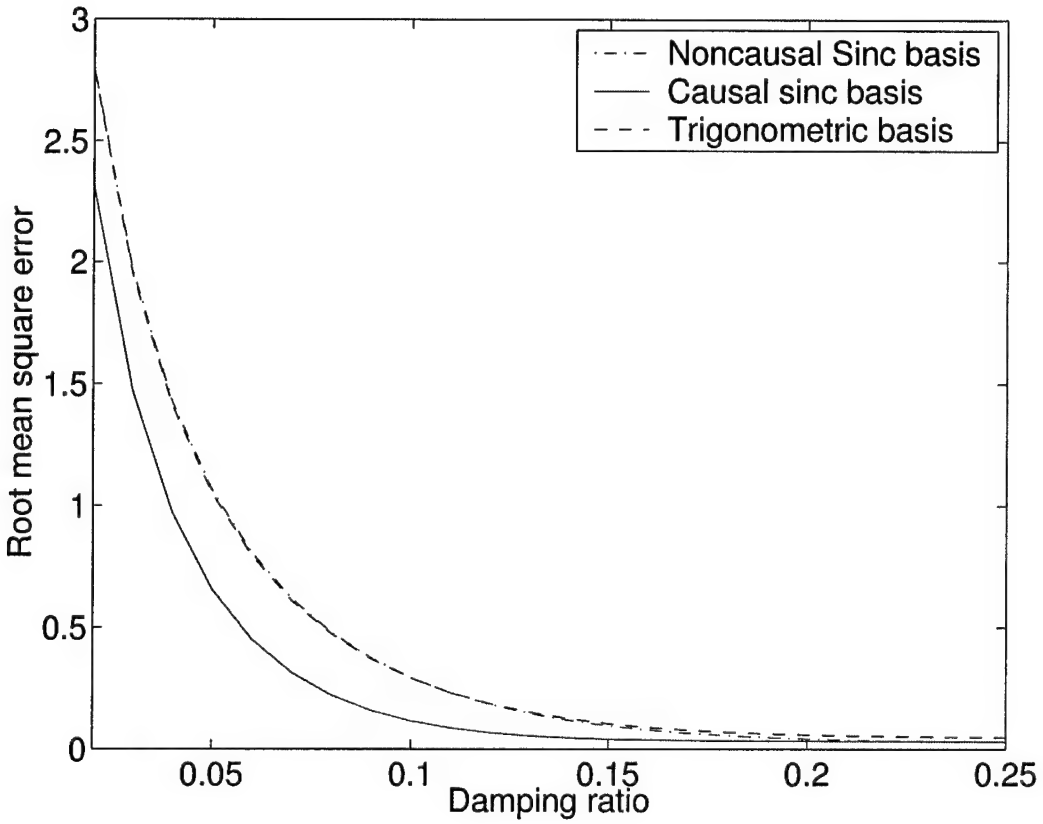

Figure 7.9: Root mean square errors from there different interpolation bases versus the damping ratio.

7.4.2 Transmission tower example

In this example, we use a finite element model of a transmission tower from the Harwell-Boeing matrix collection. The original numerical model does not include a damping matrix. For the purpose of our investigation, a non-proportional damping matrix is added to the model by the following equation

$$\mathbf{C} = 0.0002\mathbf{K} + 40\|\mathbf{M}\|_2\mathbf{D}, \tag{7.28}$$

where $\mathbf{D}$ is a randomly generated diagonal matrix and $\|\mathbf{M}\|_2$ is the 2-norm of the mass matrix. Here the damping matrix $\mathbf{C}$ includes two parts; one is the proportional damping term $0.0002\mathbf{K}$, the other is the non-proportional damping term $40\|\mathbf{M}\|_2\mathbf{D}$.

The exact transfer function of the structure from 0 to 400 rad/s is plotted together with the sampled points in the first plot of Fig. 7.10. The function is sampled with a spacing of 5 rad/s apart and the interpolation is carried out using the causal sinc basis. The corresponding impulse response and the temporal truncation due to the samples is illustrated in the second plot of Figure 7.10. As discussed before, the interpolation error is affected by the temporal truncation. At this sampling rate, the temporal truncation is small. Therefore, the interpolation errors of both magnitude and phase angle as shown in Figure 7.11 are negligible. The causal sinc basis tends to produce larger errors near the boundary region, but has greater accuracy in the interior frequency range. The error goes to zero at each sampled point indicating the interpolation matches the transfer function at each sample.

After we inrease the frequency spacing to 10 rad/s, we find that the temporal truncation moves towards the center of the coordinate, as shown in Figure 7.12). Due to this movement, the error gets larger but is still reasonable, as shown in Figure 7.13. For the case when the frequency spacing is 20 rad/s, we find that the truncation is significant in the time domain, as shown in Figure 7.14. The results shown in Figure 7.15 are not as accurate as before.

To clarify the relationship between temporal truncation and the interpolation accuracy, we tried several other frequency spacings and plotted the RMS error with respect to the integral of temporal truncations, $\int_{t>2T} |h(t)|dt$, in Figure 7.16. It shows an increasing error as temporal truncation increases. However, it is more irregular than might be expected, because the series truncation also contributes to the error as discussed in Section 7.3.2.

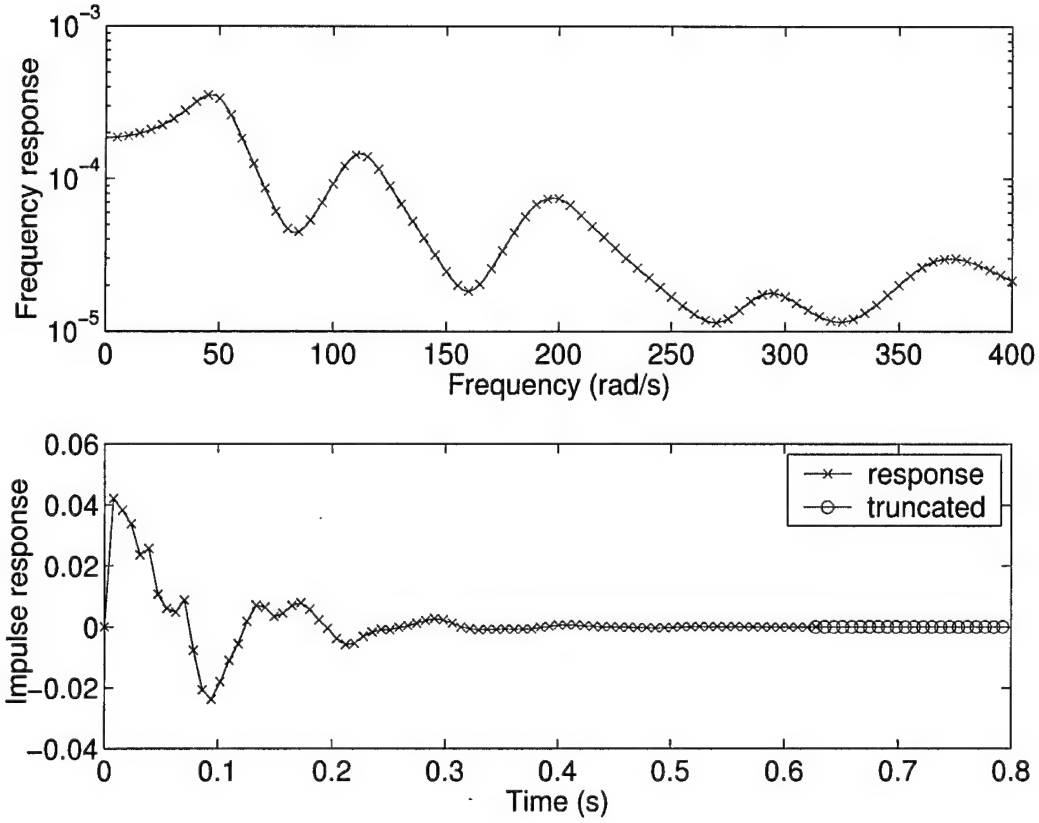

Figure 7.10: Exact transfer function with frequency spacing of 5 rad/s in the upper plot. The sampled points are shown by the cross mark. The corresponding impulse response is shown in the lower plot together with the temporal truncation.

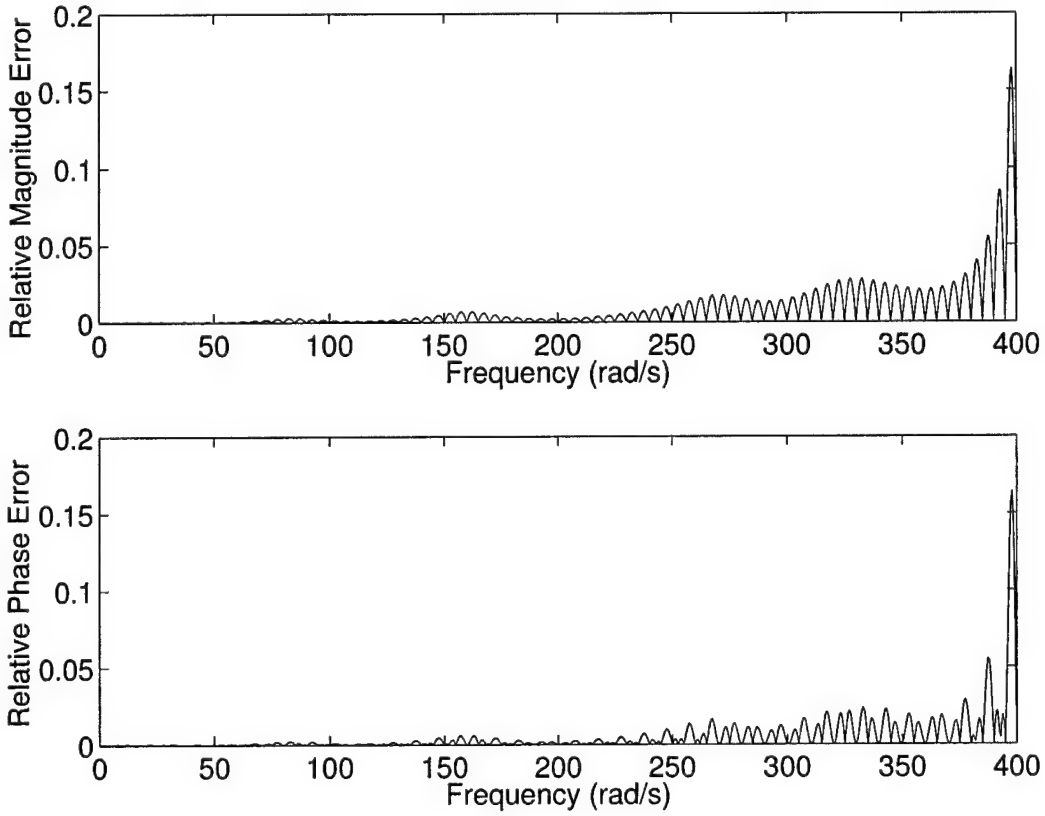

Figure 7.11: Error of magnitude and phase angle with frequency spacing of 5 rad/s.

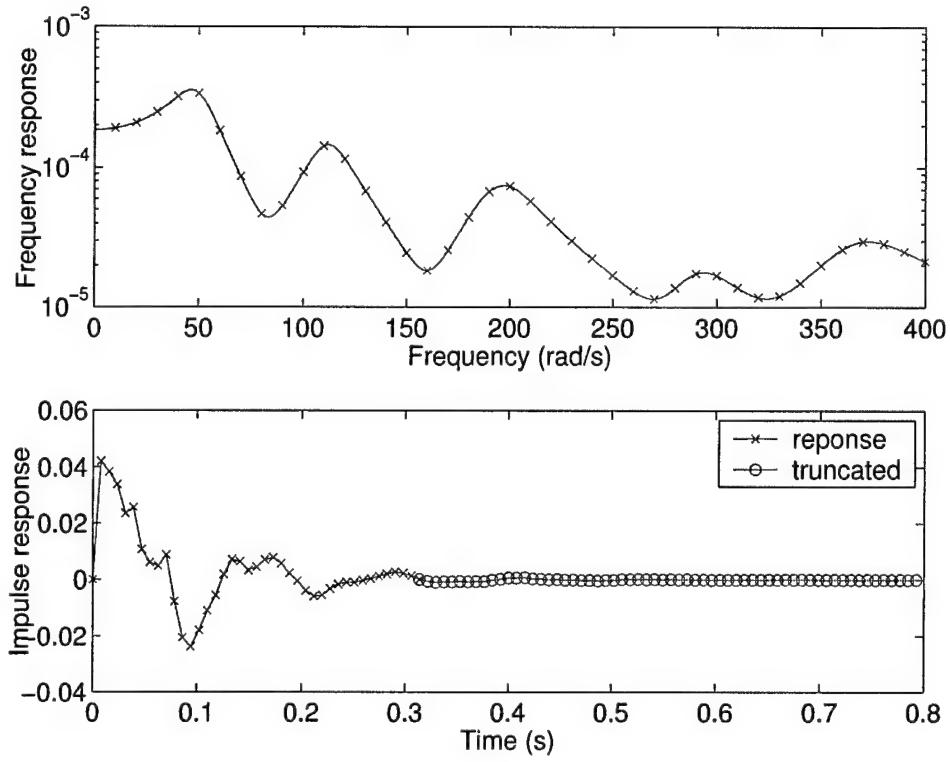

Figure 7.12: Exact transfer function with frequency spacing of 10 rad/s shown in the upper plot. The sampled points are shown by the cross mark. The corresponding impulse response is shown in the lower plot together with the temporal truncation.

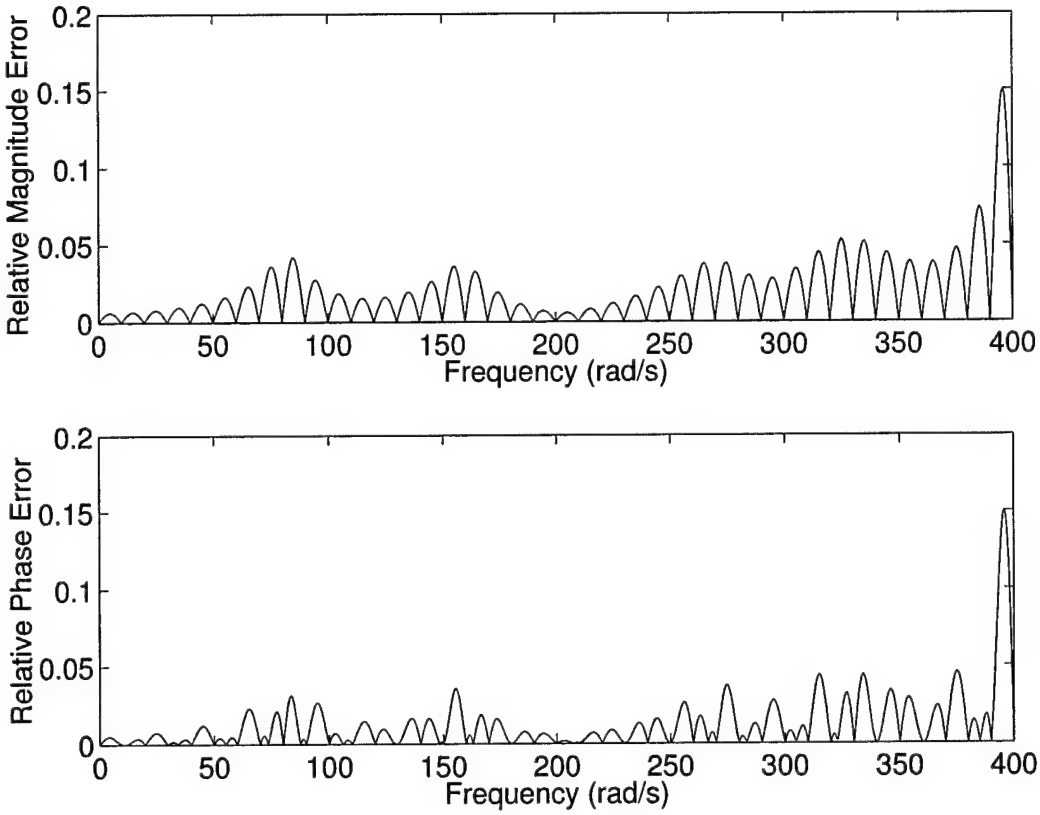

Figure 7.13: Error of magnitude and phase angle with frequency spacing of 10 rad/s.

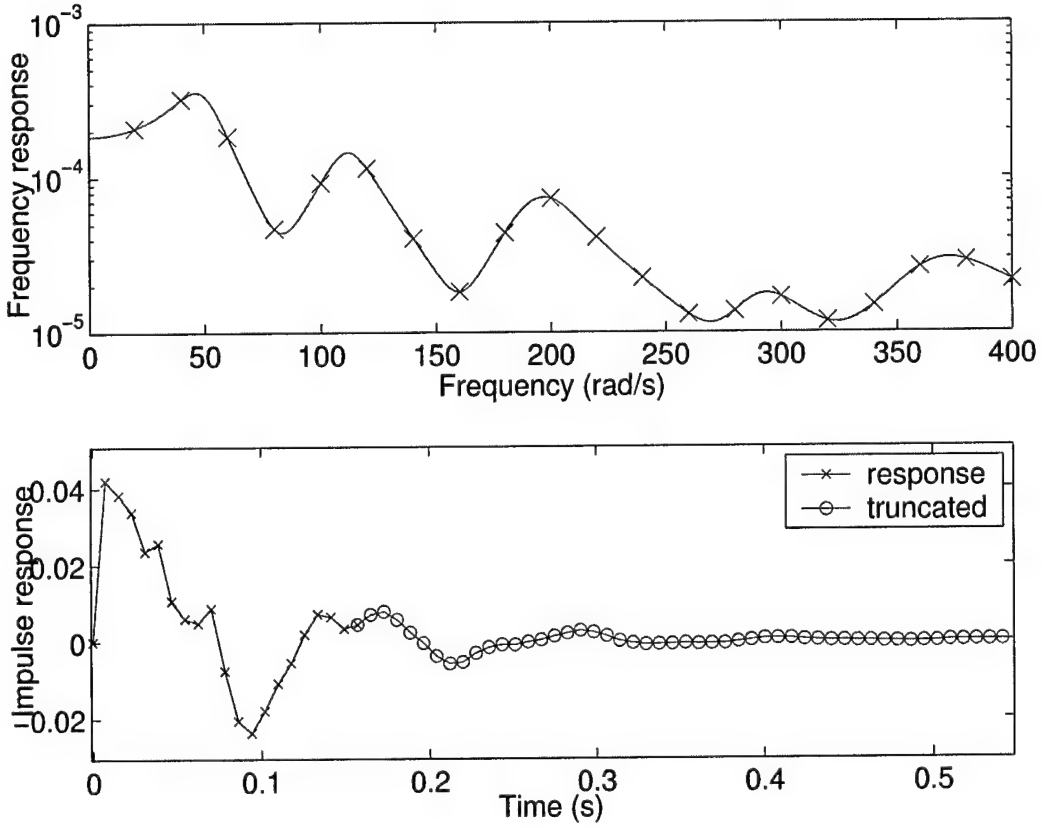

Figure 7.14: Exact transfer function with frequency spacing of 20 rad/s shown in the upper plot. The sampled points are shown by the cross mark. The corresponding impulse response is shown in the lower plot together with the temporal truncation.

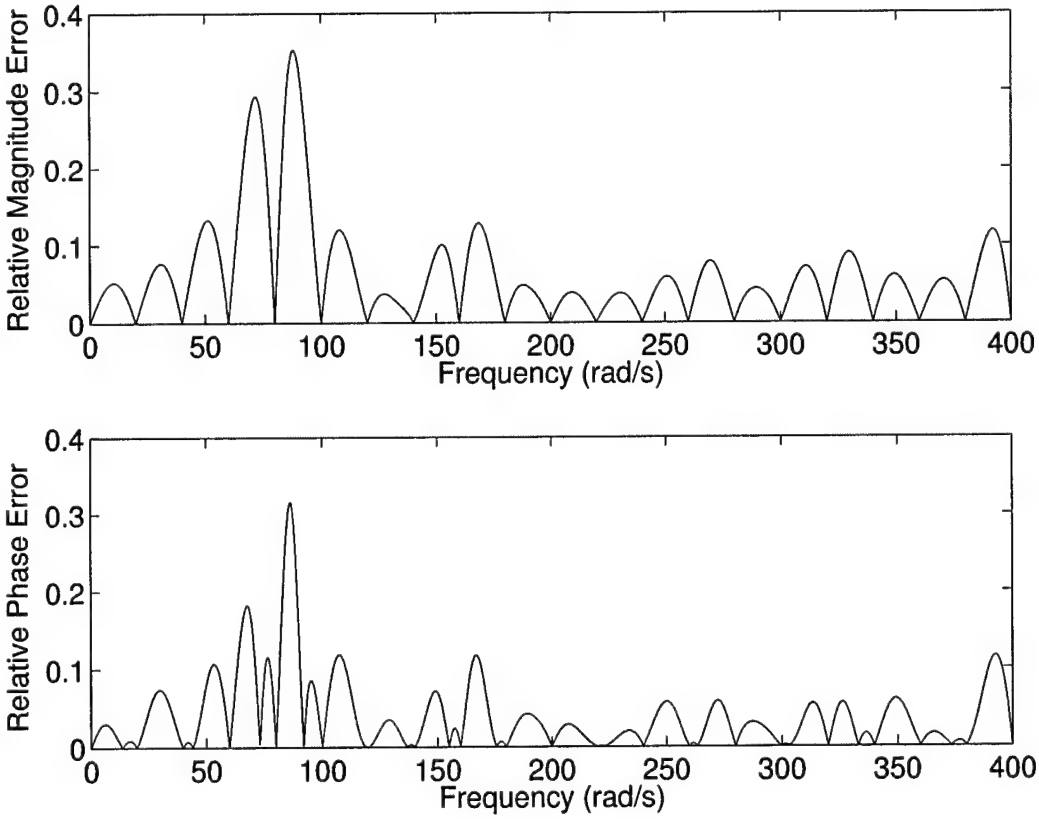

Figure 7.15: Error of magnitude and phase angle with frequency spacing of 20 rad/s.

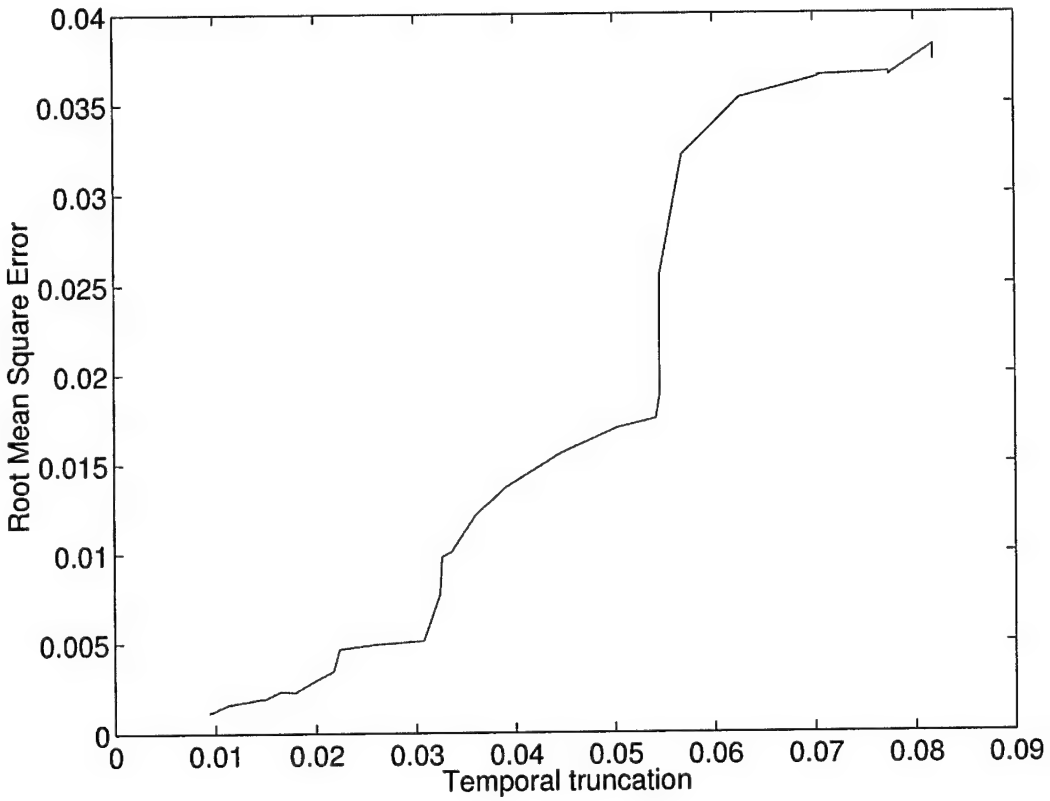

Figure 7.16: Root mean square curve with respect to the integral of the truncated time domain signal.

Chapter 8

Conclusions

This project has successfully investigated an analytical framework for satisfying the causality condition in analysis and active control. A fundamental conclusion of this work is that the causality condition can be implicitly satisfied by causal expansions of transfer functions. Each basis function in a causal expansion obeys the Hilbert transform relations. In many cases, we have found that trigonometric functions make a mathematically convenient and appealing choice. Regardless of the choice of basis function, this framework offers a causal mapping between measured or desired values of a transfer function and values at other frequencies.

From this analytical framework, previously noncausal control approaches may be made causal with very little loss in performance. This was demonstrated for two control approaches: maximum power absorption and minimization of net power in. Phase noise may be removed from measurements by finding the causal transfer function that best approximates the data, as demonstrated on the rich and challenging dataset provided by NRL. Transfer functions may be interpolated so that the interpolated function is causal, which is much more appealing than purely numerical approaches that violate causality. The phase of a reflected wave may be determined from the more easily measured magnitude if the reflection coefficient is minimum phase.

This work represents much more than a simple check to determine if a model or set of data satisfies the causality condition. Instead, it offers a means of determining unmeasured quantities from applying Hilbert transform relations to measured quantities and correcting experimental errors. Using the same analytical framework allows one to find power absorbers that achieve global reductions in sound and vibration for transient disturbances. Our initial investigations have discovered and illustrated these concepts. We expect even more impressive results as they find applications in the Navy research and development community.

Chapter 9

Publications and Presentations

9.1 Publications

The project produced the following publications:

- "Simplified dynamics models of submerged objects from limited scattering data," J. Gregory McDaniel and Cory L. Clarke, Proceedings of the 2001 ASME International Mechanical Engineering Congress and Exposition, New York, NY, November 2001.
- "Interpretation and identification of minimum phase reflection coefficients," J. Gregory McDaniel and Cory L. Clarke, The Journal of the Acoustical Society of America, Vol. 110, No. 6, pp. 3003-3010, December 2001.
- "Applications of the Causality Condition to Mechanical Impedances and Acoustic Reflection Coefficients with Minimum and Nonminimum Phases," Cory L. Clarke, Master's Thesis, Aerospace and Mechanical Engineering Department, Boston University, December 2000.
- "Interpolation of Transfer Functions for Damped Vibrating Systems," Xianfeng Zhao, Chapter 4, Ph.D. Thesis, Aerospace and Mechanical Engineering Department, Boston University, June 2004.
- "Numerical Evaluation of the Hilbert Transform," Boston University Technical Report, October 1999.

9.2 Presentations

The project produced the following presentations:

- "Causal Boundaries for Structural Acoustic Analysis and Design," J. Gregory McDaniel, presented at the George W. Woodruff School of Mechanical Engineering, Georgia Institute of Technology, July 17, 2002. 4.
- "Causal Frequency-Domain Searches for Improved Data, Designs, and Controllers," J. Gregory McDaniel and Cory L. Clarke, presented at the Structural Mechanics, Computational Mechanics, and Acoustic Signatures FY2002 Program Review, sponsored by the Office of Naval Research, April 18, 2002.
- "Causality applied to the acoustic identification of submerged objects in noisy environments," J. Gregory McDaniel and Cory L. Clarke, presented at the Structural Mechanics, Computational Mechanics, and Acoustic Signatures FY2001 Program Review, sponsored by the Office of Naval Research, April 26, 2001.

- "Applications of the causality condition to acoustic sensing in noisy environments," presented to the Center for Subsurface Sensing and Imaging Systems (CENSSIS), Northeastern University, March 9, 2001. 7.
- "Applications of the causality condition to acoustic sensing in noisy environments," presented at the Department of Mechanical, Industrial, and Manufacturing Engineering, Northeastern University, January 26, 2001
- "Recent results on causality applications and the vibrations of complex structures," J. Gregory McDaniel, presented at Electric Boat in Groton, Connecticut on July 10, 2000.
- "Estimating reflection coefficient phase from measured magnitude using the causality condition," J. Gregory McDaniel and Cory L. Clarke, presented at the Structural Mechanics, Computational Mechanics, and Acoustic Signatures FY2000 Program Review, sponsored by the Office of Naval Research, May 24, 2000.
- "Some emerging structural acoustic technologies: causality and the vibrations of complex structures," J. Gregory McDaniel and Cory Clarke, presented at Newport News Shipbuilding in Newport News, Virginia on April 28, 2000.

The project also provided material for Boston Universitys Pathways 2000 program, which inspires women in science and engineering .

Chapter 10

Future Work

10.1 Design Methodologies

This work has yielded analytical formulations for constructing dynamic representations, such as impedance and admittance, that satisfy causality and minimum phase requirements. If further developed, these formulations are capable of yielding conceptual design tools for investigating the optimization of complex structural acoustic systems. The envisioned approach would yield indicate optimal and causal admittance matrices for achieving structural acoustic performance by using

- Representation of drive-point admittances by implicitly causal and minimum phase frequency expansions.
- Representation of transfer admittances by implicitly causal frequency expansions.
- Optimization of structural acoustic performance over all Fourier harmonics.
- Methodologies to achieve optimized admittance matrices active and passive design technologies.

10.2 Time Separation

Our interactions with Newport News Shipbuilding have identified an important future direction of the work. In brief, structural acoustic testing of ship structures often involves acoustic radiation from several discrete portions of the wetted surface. Radiation from each portion arrives at a hydrophone at a time determined by the sound speed and the distance from that portion and the hydrophone. Since the radiating portions are typically different distances from the hydrophone, the arrivals are separated in time but often overlapping. The PI has met with staff at Newport News Shipbuilding to determine if concepts developed in this project can be further developed to allow for the complete separation of the separate arrivals.

Chapter 11

Acknowledgements

We are very grateful to the Office of Naval Research for supporting the project. We acknowledge the help of the following individuals who offered technical advice and encouragement during the course of the research (in alphabetical order):

- Willliam Carey, Boston University
- Robin Cleveland, Boston University
- Luise Couchman, ONR
- Pierre Dupont, Boston University
- David Feit, CDNSWC
- Brian Houston, NRL
- Geoffrey Main, ONR
- Allan D. Pierce, Boston University
- Ron Radlinski, ONR
- Ronald Roy, Boston University
- Steve Schreppler, ONR
- Richard Shaw, Newport News Shipbuilding
- Murray Strasberg, CDNSWC
- Jay Warren, Newport News Shipbuilding
- Kuangcheng Wu, Newport News Shipbuilding

Bibliography

[1] V. Mangulis, "Kramers-Kronig or dispersion relations in acoustics," The Journal of the Acoustical Society of America **36**(1), 211–212 (1964).

[2] R. Radlinski and T. Meyers, "Radiation patterns and radiation impedances of a pulsating cylinder surrounded by a circular cage of parallel cylindrical rods," The Journal of the Acoustical Society of America **56**(3), 842–848 (1974).

[3] J. G. McDaniel, "Hilbert transforms: Implications for structural acoustic design," in *ONR-Sponsored European Workshop on Structural Acoustics for Young Investigators* (ONR, Cambridge, England, 1993).

[4] J. G. McDaniel, "Applications of the causality condition to acoustic reflections," in *Proceedings of the 1997 ASME Design Engineering Technical Conferences, DETC97/VIB–4133* (ASME, Sacramento, California, 1997).

[5] J. G. McDaniel, "Applications of the causality condition to acoustic scattering," The Journal of the Acoustical Society of America **102**(5), 3073 (1997), 134th Meeting of the Acoustical Society of America.

[6] J. G. McDaniel, "Applications of the causality condition to one-dimensional acoustic reflection problems," The Journal of the Acoustical Society of America **105**(5), 2710–2716 (1999).

[7] J. G. McDaniel, "Simplified dynamic models of submerged objects from limited scattering data," in *ASME IMEC* (ASME, New York, 2001).

[8] J. G. McDaniel and C. L. Clarke, "Interpretation and identification of minimum phase reflection coefficients," Journal of the Acoustical Society of America **110**(6), 3003–3010 (2001).

[9] A. Papoulis, *The Fourier Integral and Its Applications* (McGraw-Hill, Inc., New York, 1962).

[10] R. N. Bracewell, "The Hilbert transform," *The Fourier Transform and Its Applications* (McGraw-Hill Book Company, New York, 1965), pp. 267–272.

[11] E. Guillemin, *Synthesis of Passive Networks* (John Wiley & Sons, Inc., New York, 1957).

[12] R. H. Lyon, "Statistics of phase and magnitude of structural transfer functions," in *Studies in Applied Mechanics*, edited by I. Elishakoff and R. Lyon (Elsevier, New York, 1986), Vol. 14.

[13] B. Kuo, *Automatic Control Systems*, sixth ed. (Prentice Hall, New Jersey, 1991).

[14] J. D. Victor, "Temporal impulse responses from flicker sensitivities - causality, linearity, and amplitude data do not determine phase," Journal of the Optical Society of America A-Optics Image Science and Vision **6**(9), 1302–1303 (1989).

[15] H. Nussenzveig, *Causality and Dispersion Relations* (Academic Press, New York, 1972).

[16] E. Eisner, "Tutorial: Minimum phase for continuous time and discrete time functions," Geophysical Prospecting **32**, 533–541 (1984).

[17] S. Hahn, "Hilbert Transforms," in *The Transforms and Applications Handbook, The Electronic Engineering Handbook Series*, 2nd ed., edited by A. D. Poularikas (CRC Press and IEEE Press, Boca Raton, 2000).

[18] T. K. Sarkar and B. Hu, "Generation of nonminimum phase from amplitude-only data," IEEE Transactions On Microwave Theory And Techniques **46**(8), 1079–1084 (1998).

[19] R. Henery, "Hilbert transforms using Fast Fourier Transforms," Journal of Physics, Series A **17**, 3415–3423 (1984).

[20] K. Howell, "Fourier Transforms," in *The Transforms and Applications Handbook, The Electronic Engineering Handbook Series*, 2nd ed., edited by A. Poularikas (CRC Press and IEEE Press, Boca Raton, 2000).

[21] E. Guillemin, *The Mathematics of Circuit Analysis* (John Wiley & Sons, Inc., New York, 1949).

[22] Pierce:1989, *Acoustics, An Introduction to Its Physical Principles and Applications* (The Acoustical Society of America, New York, 1989).

[23] J. A. Bucaro, A. J. Romano, A. Sarkissian, D. M. Photiadis, and B. H. Houston, "Local admittance model for acoustic scattering from a cylindrical shell with many internal oscillators," The Journal of the Acoustical Society of America **103**(4), 1867–1873 (1998).

[24] P. A. Nelson, J. K. Hammond, P. Joseph, and S. J. Elliott, "Active control of stationary random sound fields," Journal of the Acoustical Society of America **87**(3), 963–975 (1990).

[25] S. Elliott, P. Joseph, P. Nelson, and M. Johnson, "Power output minimization and power absorption in the active control of sound," The Journal of the Acoustical Society of America **90**(5), 2501–2512 (1991).

[26] P. Nelson and S. Elliot, *Active Control of Sound* (Academic Press, Boston, 1992).

[27] N. Hiram, "An active maximum power absorber for the reduction of noise and vibration," Journal of Sound and Vibration **200**(3), 261–279 (1997).

[28] N. Hiram, "Optimal energy absorption as an active noise and vibration control strategy," Journal of Sound and Vibration **200**(3), 243–259 (1997).

[29] C. Shannon, "Communication in the presence of noise," Proceedings of IRE **37**, 10–21 (1949).

[30] Kotel'nikov, "On the transmission capacity of the 'ether' and wire in telecommunications," in *Modern Sampling Theory: Mathematics and Applications*, edited by J. Benedetto and P. Ferreira (Birkhauser, Boston, 2001).

[31] J. Yen, "On nonuniform sampling of bandwidth-limited signals," IRE Transactions on Circuit Theory **3**, 251–257 (1956).

[32] K. Yao and J. Thomas, "On some stability and interpolatory properties of nonuniform sampling expansions," IEEE Transactions of Circuit Theory **14**, 404–408 (1967).

[33] D. Wingham, "The reconstruction of a band-limited function and its fourier transform from a nite number of samples at arbitrary locations by singular value decomposition," IEEE Transactions of Circuit Theory **40**, 559–570 (1992).

[34] M. Soumekh, "Band-limited reconstruction from unevenly spaced data," IEEE Transactions on Acoustics, Speech, and Signal Processing **36**, 110–122 (1988).

[35] M. Unser, "Sampling – 50 years after Shannon," Proceedings of the IEEE **88**, 569–587 (2000).

[36] A. Gacia, "A brief walk through sampling theory," Advances in Imaging and Electron Physics **124**, 63–137 (2002).

[37] M. Tabei and M. Ueda, "On the sampling conditions for reconstruction of an acoustic field from a finite sound source," The Journal of the Acoustical Society of America **111**, 940–946 (2002).

[38] E. Yudilevich and H. Stark, "Interpolation from samples on a linear spiral scan," IEEE Transactions on Medical Imaging **MI-6**, 193–200 (1987).

[39] T. Strohmer, "Numerical an analysis of the nonuniform sampling problem," Journal of Computational and Applied Mathematics **122**, 297–316 (2000).

[40] A. Papoulis, *Signal Analysis* (McGraw-Hill Book Company, New York, 1977).

[41] B. D. O. Anderson and M. Green, "Hilbert transform and gain phase error-bounds for rational functions," IEEE Transactions On Circuits And Systems **35**(5), 528–535 (1988).

[42] T. R. Arabi, A. T. Murphy, and T. K. Sarkar, "An efficient technique for the time domain analysis of multi-conductor transmission lines using the hilbert transform," IEEE MTT-S Digest **OF-I-10**, 185–188 (1991).

[43] N. W. Ashcroft and N. D. Mermin, "Appendix K: Optical properties of solids," *Solid State Physics* (Holt, Rinehart and Winston, New York, 1975).

[44] A. Ben-Menahem and S. J. Singh, "Appendix K: The mathematics of causality," *Seismic Waves and Sources* (Springer-Verlag, New York, 1981).

[45] H. Bode, "Relations between attenuation and phase in feedback amplifier design," Bell Systems Technical Journal **19**, 421–454 (1940).

[46] H. Bode, *Network Analysis and Feedback Amplifier Design* (D. Van Nostrand Company, New Jersey, 1945).

[47] H. W. Bode, "Amplifier," U.S. Patent Number 2,123,178, (1938).

[48] G. Caviglia and A. Morro, "Causality and solvability of reflection-transmission problems," Meccanica **32**(4), 301–314 (1997).

[49] C. L. Clarke, "Applications of the causality condition to mechanical impedances and acoustic reection coefficients with minimum and nonminimum phases," Master's Thesis, Boston University, 2001.

[50] A. R. D. Curtis, P. A. Nelson, and S. J. Elliott, "Active reduction of a one-dimensional enclosed sound field - an experimental investigation of 3 control strategies," The Journal of the Acoustical Society of America **88**(5), 2265–2268 (1990).

[51] E. Eisner and G. Hampson, "Decomposition into minimum and maximum phase components," Geophysics **55**(7), 897–901 (1990).

[52] E. Eisner and G. Hampson, "Decomposition into minimum and maximum phase components - reply," Geophysics **58**(8), 1208–1–213 (1993).

[53] J. D. Ferry, "Chapter 3: Exact interrelations among the viscoelastic functions," *Viscoelastic Properties of Polymers* (John Wiley & Sones, Inc., New York, 1980).

[54] J. S. Freeman, "Use of the hilbert transform in linear and non-linear modal analysis," Master's Thesis, University of Wisconsin – Madison, 1985.

[55] B. Gross, "On the theory of dielectric loss," Physical Review **59**, 758–750 (1941).

[56] N. D. Hargreaves, "Air-gun signatures and the minimum-phase assumption," Geophysics **57**(2), 263–271 (1992).

[57] J. Hilgevoord, *Dispersion Relations and Causal Description* (North-Holland Publishing Company, Amsterdam, 1960).

[58] C. Holbrow and W. Davidon, "An introduction to dispersion relations," American Journal of Physics **32**, 762–774 (1964).

[59] B. H. Houston, M. H. Marcus, J. A. Bucaro, E. G. Williams, and D. M. Photiadis, "The structural acoustics and active control of interior noise in a ribbed cylindrical shell," The Journal of the Acoustical Society of America **99**(6), 3497–3512 (1996).

[60] J. A. Inaudi and J. M. Kelly, "Linear hysteretic damping and the Hilbert Transform," Journal of Engineering Mechanics,626–632 (1995).

[61] M. T. Jaekel and S. Reynaud, "Causality, stability and passivity for a mirror in vacuum," Physics Letters A **167**(3), 227–232 (1992).

[62] J. R. James and G. Andresic, "On the use of the Hilbert Transform for processing measured CW data - Comments," IEEE Transactions On Electromagnetic Compatibility **35**(3), 408–408 (1993).

[63] P. C. Johnson, "Feasibility of using the hilbert transform to improve the estimation of frequency response functions," Master's Thesis, Michigan Technological University, 1989.

[64] S. C. Kak, "Causality and limits on frequency functions," International Journal of Electronics **30**(1), 41–47 (1971).

[65] J. Koh, Y. K. Cho, and T. K. Sarkar, "Reconstruction of non-minimum phase function from only amplitude data," Microwave and Optical Technology Letters **35**(3), 212–216 (2002).

[66] H. Kramers, "La difusion de la lumiere par les atomes," Estratto dagi Atti del Congresso Internazionale de Fisici Como **2**, 545–557 (1927).

[67] R. d. L. Kronig, "On the theory of the dispersion of x-rays," Journal of the Optical Society of America and Review of Scientific Instruments **12**, 547–557 (1926).

[68] Y. Lee, "Synthesis of electric networks by means of the Fourier Transforms of Laguerre's functions," Journal of Mathematics and Physics **11**, 83–113 (1932).

[69] N. Levinson, "Simplified treatment of integrals of Cauchy type, the Hilbert problem and singular integral equations. appendix: Poincaré-Bertrand formula," SIAM Review **7**(4), 474–502 (1965).

[70] J. R. MacDonald and M. K. Brachman, "Linear-system integral transform relations," Reviews of Modern Physics **28**(4), 393–422 (1956).

[71] M. A. Muriel and A. Carballar, "Phase reconstruction from reflectivity in uniform fiber bragg gratings," Optics Letters **22**(2), 93–95 (1997).

[72] K. Naghshineh, W. C. Chen, and G. H. Koopmann, "Use of acoustic basis functions for active control of sound power radiated from a cylindrical shell," Journal of the Acoustical Society of America **103**(4), 1897–1903 (1998).

[73] R. E. Paley and N. Wiener, "Fourier Transforms in the complex domain," American Mathematical Society Colloquium Publications **XIX**, 14–25 (1934).

[74] D. Pastor and J. Capmany, "Experimental demonstration of phase reconstruction from reflectivity in uniform fibre Bragg gratings using the Wiener-Lee transform," Electronics Letters **34**(13), 1344–1345 (1998).

[75] P. A. Perry and T. J. Brazil, "Forcing causality on s-parameter data using the hilbert transform," Ieee Microwave And Guided Wave Letters **8**(11), 378–380 (1998).

[76] R. Piringer, "Equivalence of different relations between attenuation and phase," Acta Technica Csav **5**, 487–490 (1972).

[77] T. F. Quatieri and A. V. Oppenheim, "Iterative techniques for minimum phase signal reconstruction from phase or magnitude," IEEE Transactions on Acoustics, Speech, and Signal Processing **ASSP–29**(6), 1187–1193 (1981).

[78] G. Raisbeck, "A definition of passive linear networks in terms of time and energy," Journal of Applied Physics **25**(12), 1510–1514 (1954).

[79] J. G. Saha, C. H. Mehta, and S. Benjamin, "Decomposition into minimum and maximum phase components," Geophysics **58**(8), 1207–1208 (1993).

[80] R. Scanlan, "Linear damping models and causality in vibrations," Journal of Sound and Vibration **13**(4), 499–509 (1970).

[81] M. Shi, Z. Chen, and J. Sun, "Kramers-Kronig transform used as stability criterion of concrete," Cement and Concrete Research **29**, 1685–1688 (1999).

[82] P. P. Singh and W. J. Thompson, "Exploring the complex plane: Green's functions, Hilbert transforms, and analytic continuation," Computers in Physics **7**(4), 388–392 (1993).

[83] J. Skaar and H. E. Engan, "Phase reconstruction from reflectivity in fiber bragg gratings," Optics Letters **24**(3), 136–138 (1999).

[84] F. Terman, *Radio Engineer's Handbook* (McGraw-Hill Book Company, New York, 1943).

[85] F. M. Tesche, "On the use of the Hilbert transform for processing measured CW data," IEEE Transactions on Electromagnetic Compatibility **34**(3), 259–266 (1992).

[86] N. Thrane, "The Hilbert transform," Bruel and Kjær Technical Review **3**, 3–15 (1984).

[87] M. Tohyama, R. H. Lyon, and T. Koike, "Reverberant phase in a room and zeros in the complex frequency plane," Journal of the Acoustical Society of America **89**(4), 1701–1707 (1991).

[88] J. S. Toll, "Causality and the dispersion relation: Logical foundations.," Physical Review **104**(6), 1760–1770 (1956).

[89] A. Trakhtman, "Hilbert oscillations and Hilbert spectra," Telecommunications and Radio Engineering, Part 2 **24**, 59–65 (1969).

[90] N. Van Kampen, "S-matrix and causality condition. I. Maxwell field," Physical Review **89**(5), 1072–1079 (1953).

[91] D. F. Williams and B. K. Alpert, "Characteristic impedance, power, and causality," IEEE Microwave and Guided Wave Letters **9**(5), 181–182 (1999).

[92] T. T. Wu, "Some properties of impedance as a causal operator," Journal of Mathematical Physics **3**(2), 262–271 (1962).

[93] B. Yegnanarayana and A. Dhayalan, "Noniterative techniques for minimum phase signal reconstruction from phase or magnitude," in *Proceedings of the ICASSP 83. IEEE International Conference on Acoustics, Speech and Signal Processing* (IEEE, Boston, 1983), Vol. 2, pp. 639–642.

[94] D. Youla, L. Castriota, and H. Carlin, "Bounded real scattering matrices and the foundations of linear passive network theory," IRE Transactions on Circuit Theory **6**, 102–124 (1959).